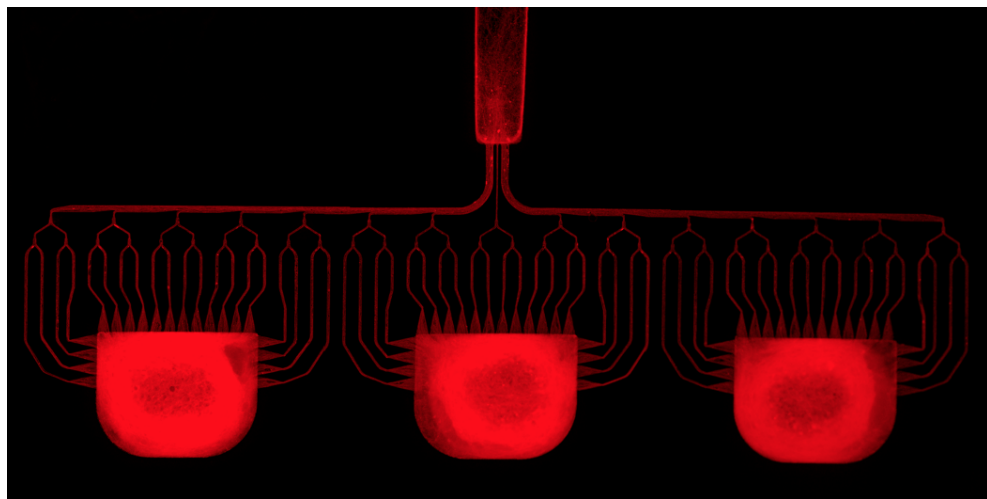


Master Thesis in Biomedical Engineering

**Restoring vision: Assembly of a stretchable
multi-electrode-microstructure composite device
optimized for axonal growth and neuronal
viability**



Eylül Ceylan

Born September 7, 1998

ETH student number: 19-950-361

February 2020 - August 2021

handed in on 2 August 2021

Advisor:
Prof. Janos Vörös

Supervisors:
Dr. Tobias Ruff
Léo Siflinger

Abstract

43.3 million people are affected by irreversible blindness worldwide as a result of conditions such as glaucoma, age-related macular degeneration (AMD), diabetic retinopathy and retinitis pigmentosa (RP). Stretchable electronics provide better conformal match with the implanted tissue thus less risk of rejection whereas biohybrid implants are a novel approach to house cultured cells in electronics in an attempt to improve biological integration. Both approaches are promising to fabricate implants that are stable in long term. The aim of this project to to assemble a stretchable biohybrid implant with axon guiding PDMS microstructures to achieve precise and selective stimulation of the dLGN tissue potentially restoring vision. Firstly, the dilution of the PDMS in hexane was optimised to obtain a thin film of glue in order to be able to bond the PDMS microstructures on top of the electrodes achieving refined axonal growth without clogging the micro-channels. Later, combinations of different coating strategies of PDMS were investigated to optimise the axonal growth in the final device. The metrics used to quantify the axonal growth are filling of the channels are with axons, surface area covered by the axons, how far the axons travel in the output channel and bundling. In the last step, a precise alignment method was developed in order to glue and seal the microstructures on top of the electrodes tracks. The optimal dilution that would reproducibly confine axonal growth without clogging the channels was found to be 1:40 PDMS:Hexane. Moreover, the ideal coating strategy was chosen to be PDL and laminin coating by desiccation after the gluing of the PDMS microstructures on top of the electrodes. The feasibility of aligning and gluing of the PDMS micro-structures on top of MEA tracks using an alignment set-up has been demonstrated. In order to further improve the cell confinement around the electrode pads, the electrode pads can be better embedded by patterning selective openings through a photoresist lift-off technique during the fabrication process. The final assembly of the stretchable microstructure-MEA device that resembles the conventional MEAs and will be used for the electrical stimulation experiments.

Acknowledgments

I would like to express my great gratitude to my supervisors Dr. Tobias Ruff, Léo Siflinger and my advisor Prof. Janos Vörös for their significant guidance and advice during this highly multidisciplinary project, helping me to gain invaluable new skills and knowledge. I would also like to thank you for being always available to answer my questions and doubts as well as sharing their expertise knowledge in the fascinating and promising field of stretchable electronics and biohybrid implants which motivated me to further explore advances in these innovative research fields. Thank you Tobias for always being enthusiastic, giving me the opportunity to work on such an exciting project, all the discussions as well as all the new knowledge and skills I've learnt in this field. Thank you Léo for all the help and advice as well as teaching me the basics of microfabrication and working in a clean room. I would like to sincerely thank Janos for all the valuable input and discussions for the project as well as career advice.

Thanks to Anna, Simon and Margherita for the team work, it was great working with you! Thanks Annina for being the best desk buddy and all the valuable input with image analysis. Jens and Stephan, thank you for all the advice, feedback and discussions about the project and image analysis, as well as trusting me with inkubot to take the cells on a road trip to ScopeM. Thank you Sophie and Ariana for the atto donations and valuable discussions! Also, thanks Sean for all the help with CLSM and practical suggestions. I would like to say thank you to all the members of the LBB family for an amazing 6 months in such a nice environment. I would also like to thank Dr. Tobias Schwarz for all the help and advice with imaging and the custom set-up.

Big thank you to my flatmates Charlotte, Claudia, Kai, Jacob, Johannes and Thibault as well as my friends Gizem, Augustina and Didem for all the encouragement and help! I would like to thank my cousins, Ilden, Elcan, Vural, Fatma, Jale and Laden for being inspiring role models. Lastly, I am extremely grateful to my family, my mother Gulter, my dad Ibrahim and my brother Ekin for their continuous support and help!

Contents

Nomenclature

Abbreviations

<i>RGC</i>	Retinal Ganglion Cell
<i>LGN</i>	Lateral Geniculate Nucleus
<i>MEA</i>	Microelectrode Array
<i>PR</i>	Photoreceptor
<i>AMD</i>	Age-related Macular Degeneration
<i>RP</i>	Retinitis Pigmentosa
<i>PDMS</i>	Polydimethylsiloxane
<i>CLSM</i>	Confocal Scanning Laser Microscope
<i>PDL</i>	Poly-D-Lysine
<i>AAV</i>	Adeno-associated virus
<i>FBR</i>	Foreign body reaction
<i>DBS</i>	Deep Brain Stimulation
<i>ECM</i>	Extracellular matrix

Chapter 1

Introduction

1.1 Vision: How do we see?

Light is an electromagnetic wave (400-700 nm) moving in waves and enters the eye through the pupil where the amount of light entering the eye can be controlled by the dilation or constriction iris. Cornea, transparent part of the eyeball that refracts light onto the lens. Lens which is a structure enclosed in a thin transparent capsule has the function of focusing light onto the retina on fovea where densely packed photoreceptor cells photons of light are converted to neural signals that is a visual depiction of the world. [?]

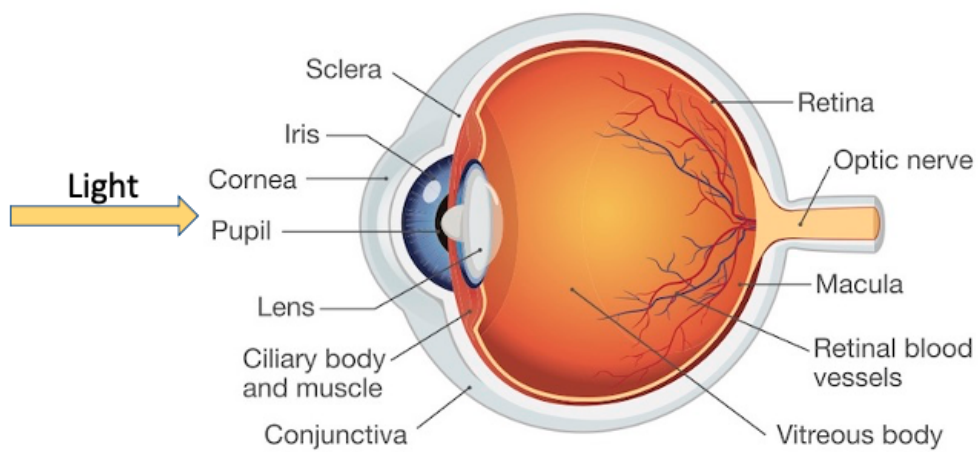


Figure 1.1: The schematic diagram of the eye anatomy [?]

1.1.1 Retina

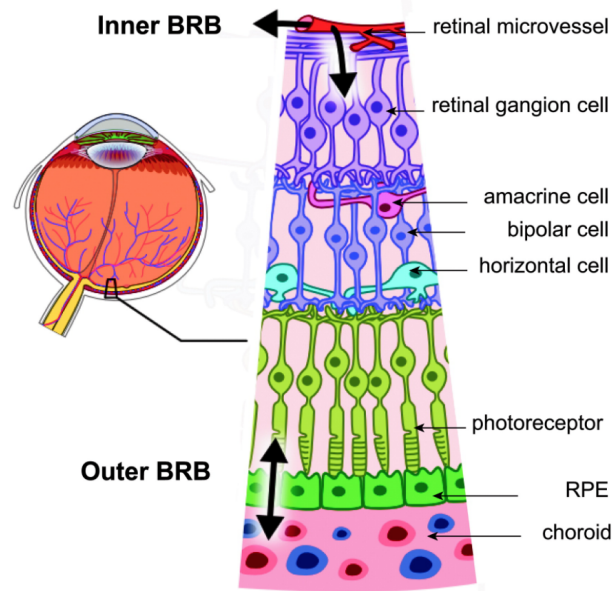


Figure 1.2: The nervous structure of retina .[?]

The fundamental pre-processing of visual information takes place at the complex neural circuitry of the retina [?]. As depicted in Figure 1.1, the retina is comprised of five main cell types as photoreceptor cells as rods and cones, horizontal cells, bipolar cells, amacrine cells and retinal ganglion cells. The photoreceptor cells are the light sensitive cells involved in the first step of vision where the captured light is converted into electrical signals in a process known as phototransduction [?]. These cells are divided into two types as cones and rods which are situated at the back of the retina adjacent to a cell layer called retinal pigment epithelium (RPE) which is essential for the survival of photoreceptors [?]. Rods are very sensitive to light and are responsible for scotopic vision since they can operate under dim light conditions whereas cones are responsible for colour vision as well as visual acuity and require bright light conditions [?]. When a photon interacts with the retinal in a photoreceptor, phototransduction is initiated. Firstly, 11-cis-retinal chromophore of rhodopsin is isomerised to all-trans configuration and results in a conformational change activating a cascade of molecular events that trigger phototransduction leading to hyperpolarisation of the nerve cell thus generation of an action potential [?]. After phototransduction, the nerve signal is further transmitted to the intermediate layer of retina which consists of mainly bipolar cells which are connected to other cell types such as amacrine cells that regulate signals directed at RGCs and horizontal cells that regulate signals from several rods and cones [?]. Later on, RGCs in the uppermost layer collect and integrate signals relayed from the bipolar cells. The complex circuitry of the neural network of cells in retina encodes for visual information such as light intensity, contrast, colour and spatial details. RGC axons eventually converge and bundle up forming the optic nerve which relays the action potentials encoding for the visual data to the brain in multiple parallel channels [?].

1.1.2 Signal Transmission to the Visual Cortex

The axon bundles from the central macular zone of the retina decussate at the optic chiasm whereas the axons projecting laterally from the temporal half of the retina remain uncrossed at target locations. The RGCs axons are guided by different axon guidance molecules along the pathway towards their original target at the optic chiasm midline [?]. By this partial-crossing, the visual information between the right and left eye is segregated where the information from the right visual field is transmitted to and processed the left side of the brain and vice versa. The field of view from each eye is processed by the opposite cerebral hemisphere meaning that the field of view from the left eye is processed on the right side and field of view of the right eye is processed on the left side of the brain. [?].

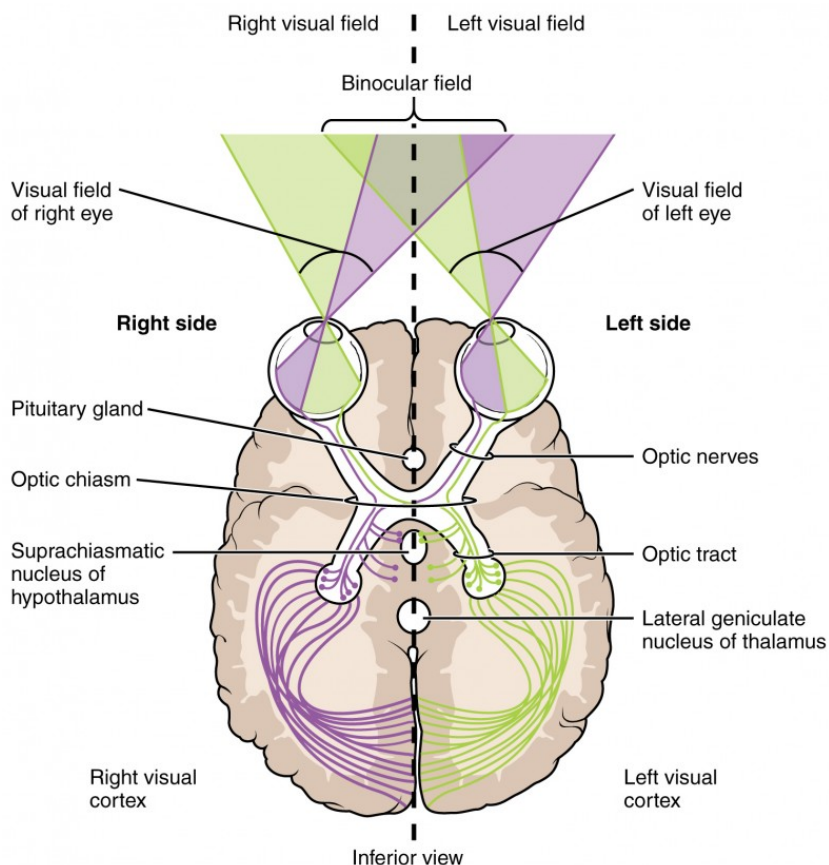


Figure 1.3: The Visual Pathway. [?]

Beyond optic chiasm, axon fibres are referred to as optic tract and further relay information to the central part of visual signal processing known as the lateral geniculate nucleus (LGN) which is located in the thalamus. Later, action potentials from LGN are transmitted via axons projecting to the visual cortex of cerebrum at the corresponding side of the brain.

1.1.3 Visual Processing and Perception

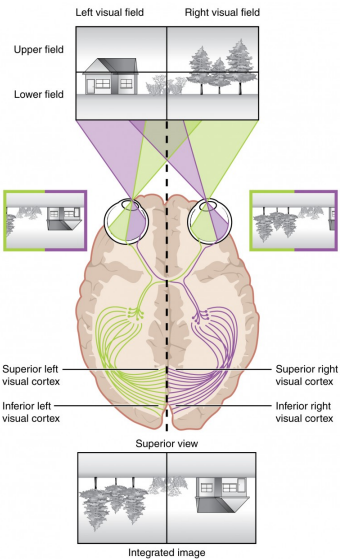


Figure 1.4: The visual processing in the visual cortex. [?]

The information received by the eyes are later decoded and translated in order to understand the properties of the physical environment and perceive the world around us via complex brain circuits in the visual cortex. Since the light first passes through the lens, the projection of the visual field on retina is inverted and reversed as shown in Figure ???. Visual stimuli is processed and mapped where the edges of shapes are recognised to understand complex shapes. Moreover, distance of the stimuli can be estimated based on binocular depth cues due to overlapping field of view of both eyes. Obtained information later helps to learn patterns which are later applied in life and base decisions on [?].

1.2 Causes of Blindness and Impact of Vision Loss

43.3 million people are affected by blindness worldwide [?] with increasing prevalence with aging population [?]. Glaucoma, age-related macular degeneration (AMD), diabetic retinopathy and retinitis pigmentosa (RP) are among the leading causes of irreversible blindness [?]. AMD is a neurodegenerative condition which causes progressive loss of photoreceptor cells in macula located in the central part of retina which leads to the loss of central vision and blindness in advanced cases [?]. RP is a hereditary retinal disease where genetic defects affects rods, leading to loss of night vision and poor peripheral vision which gradually progresses to the central retina [?]. On the other hand, glaucoma is a group of eye conditions where an abnormally high pressure in the eye results in damage to the optic nerve eventually leading to an irreversible loss of RGCs [?]. Other conditions that affect RGCs include hereditary optic neuropathies, ischaemic optic neuropathies and demyelinating disease [?]. Moreover, vision loss can happen due to damage to the eye, optic

nerve or visual cortex as a result of a stroke, brain tumour or head trauma. [?]. Vision loss has a significant impact on blind people's quality of life, independence, mobility, mental health, social function, education and employment where even basic daily activities such as reading and driving can be a challenge. [?]. Although there are treatment options to slow down disease progression, unfortunately, there are no current treatment options to reverse profound visual loss caused by such conditions [?].

1.3 Restoring Vision - State of Art

The different approaches to restore vision include electrical stimulation of the eye, various types of visual prosthesis, regenerative medicine and tissue engineering as well as other alternative approaches.

1.3.1 Electrical Stimulation

Functional recovery of nervous tissue is usually sub-optimal despite peripheral nervous system's intrinsic regenerative ability. It's been previously shown both in animal models and patients that low-frequency electrical stimulation can help to promote axonal regeneration and enhance functional recovery after various different types of peripheral nerve injuries and surgical repairs [?]. On the other hand, electrical stimulation have been shown to be a potential efficient treatment for neurological conditions such as Parkinson's disease, epilepsy, hearing loss and chronic pain [?]. Electrical stimulation upregulates the expression of neurotrophic factors in neurones and increases growth related proteins. By this way, axon outgrowth can be accelerated as a result of ES-mediated release of neurotrophic factors. Another advantage of electrical stimulation is the possibility of increasing the stimulation current to compensate for scar tissue encapsulation of electrodes [?]. There is also previous evidence that non-invasive electrical stimulation can be a potential therapeutic approach for retinal or optic nerve diseases in order to restore or improve vision [?].

1.3.2 Visual Prostheses

The working principle of visual prosthesis is based on capturing light using a video camera where the incident light is converted to analog electrical signals which are then digitised and a portable micro-computer is used to process the image. The signals are later delivered in close proximity to stimulate RGCs or bipolar cells via a MEA interface, bypassing degenerated photoreceptors. These electrical stimulation signals elicit visual percepts and cause the patients to see flashes of light called phosphenes [?] [?]. Different technologies are classified according to the target region along the visual system that results in the most effective vision restoration which is dictated by the underlying pathophysiology. Bypassing the natural neuronal circuitry that is still functional by interfacing a region downstream in the visual pathway results in poor resolution requiring complex image processing algorithms as well as extra hardware. [?]

i) Retinal Prostheses

Retinal prosthesis can utilise the natural information processing along the visual pathway. It's been previously demonstrated in several clinical trials that retinal prostheses have the capability to partially restore functional vision. [?]

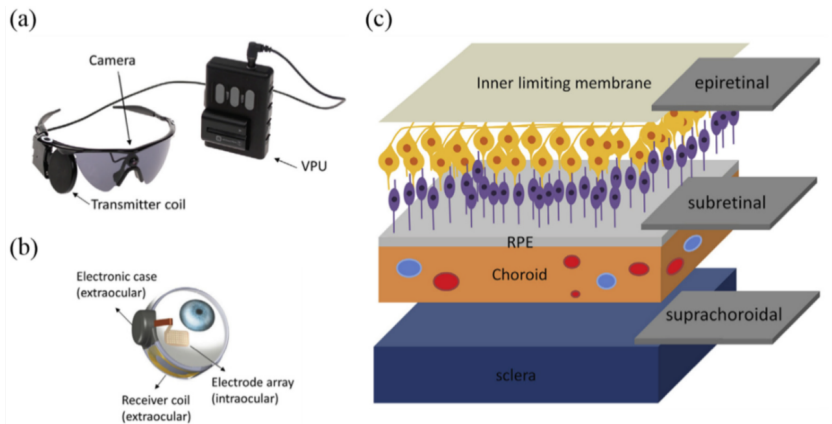


Figure 1.5: Different types of retinal implants. (a) Camera used to capture light in a retinal prosthesis. (b) Placement of the microelectrode array. (c) Different implantation sites of different retinal implants. [?]

Intraocular implants: Epiretinal Prostheses are directly implanted on top of the innermost layer of the retina and bypasses the photoreceptor cells and the intermediate layer of neural cells namely, bipolar, horizontal and amacrine. Advantage of such implants is that the device can be secured to the surface of the retina with a tack, thus the surgical operation is much less complex compared to subretinal implants. On the other hand, RGCs are more scarce compared to photoreceptors or bipolar cells allowing an accurate stimulation with inter-electrode density [?]. In addition, a safer heat dispersion occurs when the device is located in the vitreous cavity. However, stimulating the RGCs directly can be disadvantageous since the intraretinal processing will be bypassed. Last but not least, the close proximity of the epiretinal devices to the axonal nerve fibres might result in inadvertent stimulation leading to ectopic visual percepts which can negatively affect the spatial resolution. [?] Argus II Retinal Prosthesis System, Intelligent Medical Implants Learning Device/Intelligent Retinal Implant System II (IRIS), EPI-RET3 Retinal Implant System are examples of such epiretinal prostheses [?]. **Intraocular implants: Subretinal prostheses** are installed behind the retina where the device is in close proximity to the damaged photoreceptors. [?] Therefore, such implants can stimulate the bipolar cells in the retina bypassing rods and cones thus taking advantage of the intrinsic processing circuitry of the retina and require less image processing thus providing a more physiological vision. In addition, since the device is implanted in close proximity to target retina, natural signal amplification in the retina can be exploited which in turn requires lower stimulation intensities if the organisation of the retinal network is still intact. [?] One disadvantage of subretinal prosthesis is that such devices are surgically more difficult to install. Examples of such systems include Boston Retinal Implant, Artificial Silicon

Retina, Alpha IMS and AMS and Photovoltaic Retinal Implant (PRIMA) bionic vision system [?]. **Suprachoroidal Prostheses** are placed in the suprachoroidal space which makes the surgery less invasive and easily accessible for repair or replacement. One disadvantage of such implants is that there is a higher risk of haemorrhage due to the vascular structure of the suprachoroidal space and can result in fibrosis. On the other hand, due to the increased distance to the neural network of retina, a higher stimulation current is required in order to induce visual percepts. Last but not least, spatial resolution is likely to be reduced when the implant is placed in the suprachoroidal space due to the greater spread of current. [?] Examples of such devices include Bionic Vision Australia and Suprachoroidal-transretinal stimulation.

ii) Intracranial Stimulation Devices

Although current research is mostly focused on developing retinal prostheses, some research groups are attempting to develop prostheses for the stimulation of other regions of the visual pathway such as the optic nerve, visual thalamus or visual cortex [?]. **Targeting optic nerve** can be beneficial for patients with cases of retinal detachment, eyeball trauma or retinal-based diseases since stimulation of the optic-nerve bypasses the neural network in the retina and activates nerve fibres directly while still retaining the processing in the downstream visual pathway. In comparison to retinal prostheses, the signal generated after optic nerve stimulation does not depend on the complex and uncontrolled retinal processing since the axonal fibres can be selectively activated instead of cell bodies together with the neighbouring cells in the retinal network unlike retinal prosthesis. However, the downstream retinal circuitry which can provide a more physiological form of vision cannot be activated [?]. Ghezzi et al (2020) has recently reported an intraneuronal optic-nerve stimulation device, OpticSELINE for spatially selective activation of the visual cortex in rabbits. [?] **Targeting dorsal LGN (dLGN)** can generate focal percepts in response to electrical stimulation which makes it a potential target as demonstrated previously [?]. The feasibility of prostheses targeting the LGN has been proved feasible via cortical responses in animal models [?]. Object localisation tasks in primates have also shown crude resolution [?]. For patients who have either retinal or optic nerve pathologies, LGN prosthesis can be a viable and promising option for restoring vision for a number of reasons. Receptive fields in LGN are similar to retina but are simpler, well-characterised and have consistent spatial density unlike the retina [?] [?]. It is possible to achieve simple visual percepts by the stimulation of small number of LGN neurones. In addition, since 60 % of the LGN used for processing meaning that lower density MEAs can be used [?] [?]. This means mechanical insertion or delivery of stimulation current would cause less tissue damage. [?] On the other hand, LGN is adjacent to target regions for deep brain stimulation (DBS) which is used to treat conditions such as Alzheimer disease, Parkinson disease and depression via electrical stimulation of the subthalamic nucleus (STN) or globus pallidus internus (GPi) [?]. Therefore, surgical access to LGN for implantation of the electrodes can be achieved using similar techniques with a small craniotomy which will allow access to underlying visual field. [?] **Cortical prostheses** can be targeted for patients where retinal, optic nerve or LGN prosthesis will not be sufficiently effective. However, this approach has a number of limitations. Firstly, evoked percepts can differ

depending on the precise location of electrodes since the representation of visual information is highly complex in the primary visual cortex. In addition, the implantation of such stimulation devices can be complicated since the region associated with the central part of the vision can be situated deep inside the brain tissue. [?]

1.3.3 Regenerative Medicine and Cell Transplantation

Due to the limited regenerative capacity of the nervous system to proliferate and extend axons, cell transplants are also another alternative to regenerate damaged host neural tissue and restore function [?]. Such strategy would involve reprogramming cells derived from a patient in order to derive induced pluripotent stem cells (iPSCs) [?] which can later transplanted back to the injured site in the same patient (autologous transplants) [?] where the cells can integrate to the host tissue. For example, AMD has been aimed to be treated by the transplantation of RPE and photoreceptors both as suspension and scaffolds integrated with biomaterials. A recent study by Panetsos et al (2020) has demonstrated the feasibility of a silk fibroin-based biohybrid and multi-layered retina seeded with cells for use in cell replacement therapy [?].

1.3.4 Alternative Approaches

Alternative approaches to restore vision include axonal nerve guidance [?], magnetic stimulation [?] and sensory substitution [?]. On the other hand, optogenetics is a widely used technique in neuroscience that combines genetic engineering and optical technology in order to modify cells to express photosensitive proteins where light can later be utilised to manipulate biological functions [?]. In a very recent study by Sahel et al. (2021), partial recovery of functional vision of a blind patient through optogenetic therapy was reported. The patient was intraocularly injected with a AAV to transduce RGCs to express the light-gated cation channel ChrimsonR and light was detected and pulses delivered via engineered googles in order to activate the optogenetically transduced RGCs [?].

1.4 Neural Interfaces and Stretchable Electronics

MEAs are widely used for a plethora of applications such as cellular recording, drug screening, biosensors and particularly as implants as a tool for recording neural activity or restoring biological functionality as discussed previously in Section 1.3 [?]. Requirements for neural implants include well-integration, long-term stability, high resolution recording or stimulation, non-toxicity and biocompatibility. However, mechanical mismatch between rigid electronics and soft neural tissue limits the long-term stability of neural interfaces [?]. Neural tissue is subject to constant bodily motions and deformations where a rigid electronic implant can lead to a mechanical wear at the site of implant, trigger inflammatory response as well as loss of functionalities which deteriorates the performance of the implant over time, potentially leading to rejection [?] [?]. For example, scar tissue encapsulation of DBS electrodes results in increased impedance leading to a

decrease in effective range of the electrode and variation in therapeutic effects of neural excitation [?]. Therefore, conformal contact between the soft living tissue and the MEA is crucial for creating a better biological integration thus a long-term stable neural interfacing with a less risk of causing inflammatory response or loss of functionality [?] [?]. Therefore, there has been a considerable advancement in the development of soft and stretchable electronics over the recent years. Penetrating probes, stretchable or flexible neural implants as well as electrode grids have been developed to improve the electrode-tissue interface by mimicking the mechanical properties of the tissue as closely as possible for a conformal contact to the tissue while retaining their function under strain. Moreover, stretchable nature of such implants makes the insertion of implant through a smaller cranial window possible, minimising the level of invasiveness [?]. Polydimethylsiloxane (PDMS) is a prominently used substrate in the fabrication of stretchable electronics. [?] The intrinsic properties of PDMS such as optical transparency, non-toxicity, good thermal stability and high resolution with photolithography techniques as well as biocompatibility makes it an ideal substrate for stretchable electronics and biological experiments using microfluidics. Another advantage is the possibility of further functionalisation via surface modifications [?].

1.5 Biohybrid Implants

As discussed previously, cell transplantation involves providing new cells in order to replace the injured tissue whereas implantable neural interfaces can be used to either electrically stimulate or take recordings from normal healthy tissue. Both ways are considered as promising approaches to target dysfunctional neural tissue and restore normal function. However, cell transplantation and neural interfaces have been commonly considered independently [?]. One novel approach that has gained increasing attention over the recent years is referred to as biohybrid implants which aims to combine both strategies by developing implantable MEA devices which can house cultured cells. The cells within the implant can integrate into the tissue after implantation, mediating the electrode-tissue interface providing better tissue integration thus long-term stability.

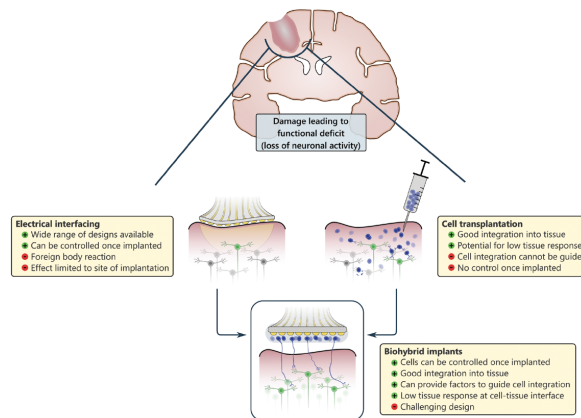


Figure 1.6: Advantages of Biohybrid Implants. [?]

FBR is one of the major challenges for long-term implants. The body elicits an inflammatory response upon implementation of such "foreign" implants in order to degrade it, leading to generation of factors such as reactive oxygen species which eventually damages the implant and the surrounding tissue. Over time, the implant becomes encapsulated and physically separated from the target tissue due to the formation of a fibrotic layer resulting in slow degradation of the electrode-tissue interface. Biohybrid implants comprise of a double-interface of electrode-cell and cell-host tissue. Therefore, due to the presence of this intermediate biological layer between the target host tissue and the electrodes, interface degradation due to FBR can potentially be minimised. On the other hand, biohybrid implants are capable of extending out from the specific site of implantation, integrating into target structures and bridging large gaps at the site of nerve damage by reestablishing lost connections. Moreover, molecular cues such as growth factors or guidance molecules can be incorporated to biohybrid implants by either fixing to the surface of the implant or delivered through microfluidic channels in order to guide and stimulate cell towards better integration of the cells to the targeted tissue. Alternatively, axon guiding structures can be incorporated to direct axonal growth. [?]. The first biohybrid approach for a regenerative neural interface was reported by Stieglitz et al. [?]. The aim of the prototype was to functionally restore and control skeletal muscle via electrical stimulation and consisted of high-channel polyimide sieve electrode, housing transplanted neurons that would act as mediators to the muscle tissue. [?].

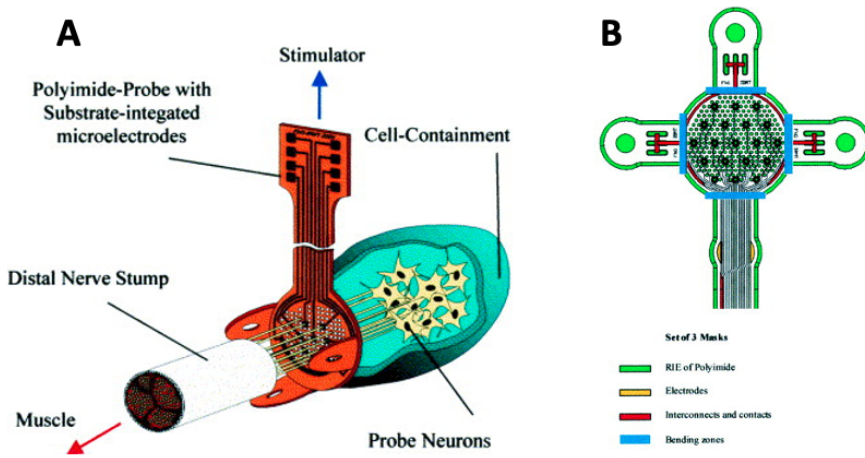


Figure 1.7: Biohybrid neural interface device by Stieglitz et al. (A) The conceptual design of the polyimide-probe device integrated with microelectrodes and transplanted cells. (B) A close-up view of the sieve area of the biohybrid implant.

There also have been reports about biohybrid implants to restore hearing and cell-seeded probes as well as electrodes combined with micro-tissue engineered neural networks (microTENN) to achieve unidirectional axonal growth. [?]. Moreover, Purcell et al. reported the design of a cell-seeded probe to better integrate the device to host tissue aiming to improve stability in long-term as well as recording quality of neurological restoration in patients with injury-related motor or

sensory impairments.[?] Despite the recent improvements in this approach, restoring vision using a biohybrid approach has yet to be described to date [?]. On the other hand, cell survival after the implantation of biohybrid implants still remains as a challenge. Coating of the electrodes should be optimised in order to improve cell attachment to electrodes and support growth of the transplanted cells in such devices. [?].

1.6 Aim of the thesis

The aim of this project is to assemble a stretchable biohybrid implant consisting of a stretchable MEA with a PDMS axon guiding microstructure to achieve precise and selective stimulation of the dLGN tissue potentially restoring vision. Firstly, a PDMS:Hexane dilution ratio will be optimised in to achieve a thin film of glue which will be used to bond the PDMS microstructure and stretchable MEA in order to refine axonal growth without clogging the micro-channels. Later, the surface coating of PDMS will be optimised in order to enhance to neuronal growth and proliferation. The metrics used to quantify the growth and proliferation performances are how filled the channels are (with axons), surface area covered by the axonal growth, how far the axons travel in the output channel and bundling. In the last step, a precise alignment method will be developed in order to glue and seal the microstructures on top of the electrodes tracks. In the final design a collagen tube for insertion of the axons to the brain and the implant will be covered with hydrogels.

Chapter 2

Materials and Methods

2.1 Micro-structure Design and Fabrication

The PDMS axon guiding micro-structures used in this project were designed in AutoCad (Autodesk, United States) and fabricated using a standard soft lithography process by Wunderlichips (Switzerland).

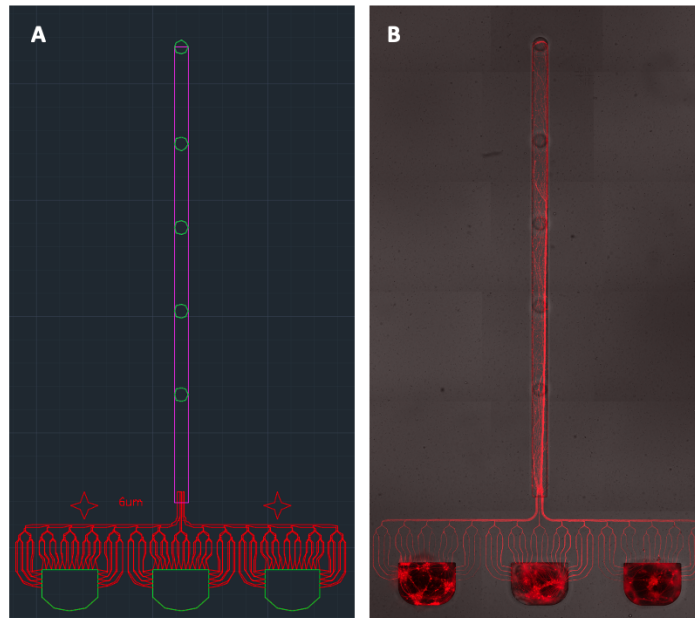


Figure 2.1: (A) CAD drawing of a 6 μm 3-well PDMS microstructure. (B) Image of the fabricated PDMS microstructure cultured with nerves.

The two types of PDMS micro-structures consists of 60 axon guiding micro-channels of width 6 or 4 μm which are shallow to prevent cell bodies moving into the channels. The micro-channels eventually merge into a single output channel of 5 mm long with a width of 150 μm . The spheroids or explants are seeded into wells of 600 μm wide.

2.2 PDMS:Hexane Glue for Bonding

In order to bond the micro-structures on the electrode surface a technique called micro-transfer assembly (μ TA) was adapted, which involves diluting PDMS in a solvent such as hexane in order to tune the thickness of the spin-coated membrane followed by stamping of the structures on the thin film of glue on the wafer as previously described [?] [?]. Glue dilution of 1:40 was previously reported to have a thickness of 373 nm characterised by AFM [?].

2.2.1 PDMS:Hexane Dilution Ratio Preparations

PDMS (prepolymer) (Sylgard 184, Dow Corning) was prepared by mixing the silicone elastomer base and curing agent at a ratio of 10:1 in a planetary mixer (2000 rpm for 3 min, defoaming at 2200 rpm for 30 secs, Thinky ARE-250). According to literature, the ratio of 10:1 is considered biocompatible for cell culture applications and provides optimum mechanical properties. [?] Different PDMS:Hexane dilution ratios of 1:25, 1:30, 1:35, 1:36, 1:37, 1:38, 1:39 and 1:40 were prepared by adding a volume of hexane (Sigma-Aldrich) for the respective dilution in a 50 mL Falcon tube. For example, to prepare a PDMS:Hexane dilution ratio of 1:40, 19.5 mL of hexane was transferred to a 50 mL falcon tube and 0.5 mL of PDMS was added. In order to be able to pipette viscous PDMS, tip of a 1 mL pipette was cut and PDMS was slowly pipetted in the stirring hexane. Residual PDMS stuck inside and on the walls of the pipette was forced out by pipetting stirring hexane up and down several times. The solution was later allowed to mix using magnetic stirrers for 5 minutes.

2.2.2 Mounting using the diluted glue

Meanwhile 3-well 6 μ m structures were cut to be glued and a clean silicon wafer was centred on the spin coater. Approximately, 1 mL of PDMS:Hexane solution was later transferred onto the wafer using a Pasteur pipette and spin coated at 2000 rpm for 60 secs with an acceleration of 300 rpm/s/s to obtain a thin membrane of glue. The structures were stamped on the thin film of glue at the edges of the spin-coated wafer and transferred on a PDMS coated petri dish after a few seconds. The structures should be mounted on the PDMS substrate by keeping the structure perpendicular to the surface to ensure sealing between the two PDMS layers. Moving the structure during or after mounting should be avoided which might otherwise clog the channels. The glued structures were cured for 2 hours at 80 °C. In addition different curing at different temperatures room temperature, 40°C and 80°C were tested. Finally, the wafer was cleaned with ethanol immediately or acetone, IPA, ultra pure water (Millipore Milli-Q System, 18M Ω) and nitrogen gun if cured. The glue dilutions were used within a few hours otherwise trashed as the evaporation of hexane over time can lead to a change in the dilution ratio. The summary of the process is illustrated in Figure ??.

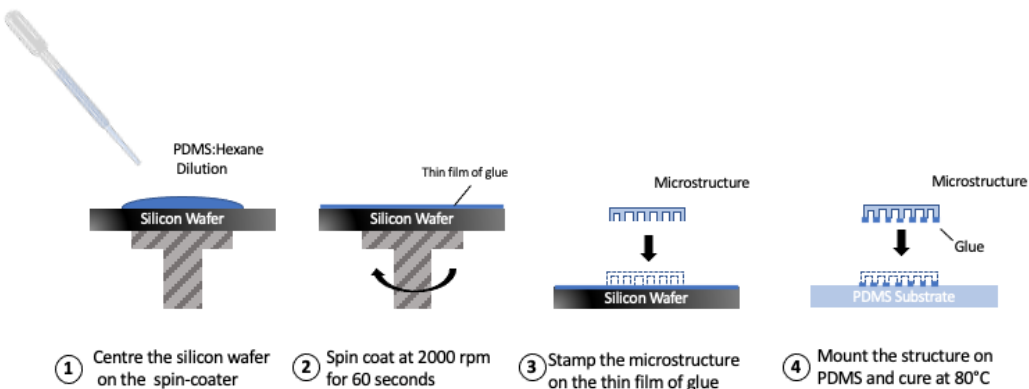


Figure 2.2: Schematic illustration of the gluing process of the microstructures.

2.2.3 Testing of the bonding for leakage and clogged channels

In order to test the glued structures for any leakage as well as for quantifying the number of open and clogged channels, a lipophilic fluorescent dye Dil, diluted in ethanol with a ratio of 10:15 was used. Imaging was performed using the Fluoview 3000 confocal laser scanning microscope (CLSM, Olympus) with a 2X and 10X lens, 2048x2048 resolution, using Alexa Fluor 647 nm. The performance and reproducibility of the bonding method in terms of cell refinement and sealing was further evaluated by cell culture experiments carried out with 44 structures with 3 different batches of the 1:40 glue dilution where the structures were examined optically using the CLSM to check for clogging and cell refinement.

2.2.4 Bonding Strength

In order to assess the bonding strength of the optimised glue dilution a T-peel test was conducted using a tensile stretching machine (Zwickline/Roell BDO-FB0.5TS, Zwick GmbH & Co.KG, Germany). Parameters of the test and the dimensions of the test strips were based on Chen et al. [?], Ohkubo et al. [?] and ISO 11339:2010 T-peel test for adhesives. In order to cut PDMS stips, PDMS substrate was prepared using the standard protocol, 24.5 g was poured into a big Petri dish to achieve a thickness of 1 mm and degassed for 10 minutes. PDMS strips of dimensions, width: 10 mm, length: 60 mm and thickness: 1mm, were prepared. Bonding was performed using three different conditions as 1:40 PDMS:Hexane glue, PDMS-PDMS and plasma bonding. 1:40 PDMS:Hexane glue dilution and PDMS were spin-coated at 2000 rpm for 60 seconds whereas plasma bonding was performed by plasma activating the surface of the strips for 2 minutes. The specimens were bonded together to form an assembly consisting of two PDMS strips with a bonding area of 40 mm X 10 mm. 20 mm from the end of the strips was left unbonded as loose ends so that samples remained slack for clamping in order to prevent initial tensile stretching. The picture of the set-up and the schematic of the test strips are given in Figure 2.2.

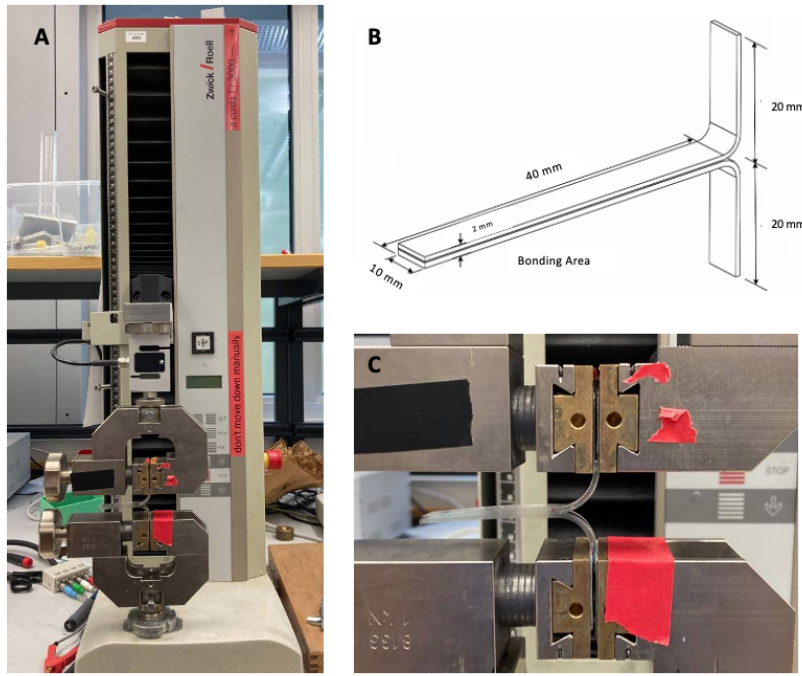


Figure 2.3: T-peel test set-up. (A) Tensile stretching machine installed with the specimen strips. (B) Dimensions of the specimen strips. (C) Close up of the installation of the test strips clamped to the machine.

T-peel test was performed by pulling the assembly of PDMS strips apart at a constant displacement rate of 60 mm/min until the strip assembly was completely pulled apart and load-extension curve was plotted to identify peak load and average force. Each condition was repeated at least 3 times. Results were later plotted as N/mm per condition.

2.3 Coating Procedures and Preparation of the Dishes

2.3.1 Preparation of Dishes

The glass bottom WillCo dishes (\varnothing 30 mm, WillCO Wells) for the control groups were assembled by using double sided adhesive (DSA) rings on the polystyrene surrounds of the dish. The glass cover slips were cleaned by rinsing with acetone, isopropanol and ultra pure water (Millipore Milli-Q System, 18M Ω) respectively, and dried with nitrogen gun. Finally, the cover slip was sealed off to the bottom of the dish. For the experimental groups, small plastic Petri dishes (\varnothing 40 mm) were coated with PDMS by adding approximately 250 μ L of PDMS to the centre of the dish without forming any bubbles, spin-coating at 1500 rpm for 60 secs and then curing for 2 hours at 80 °C. The dishes were placed inside a bigger Petri dish to make the handling easier. A strip of tape was added to the bottom of the big Petri dish in order to prevent glass bottom dishes sticking. Prior to coating, all the dishes were sterilised under UV light for 4 hours or 2 hours at 80 °C.

2.3.2 Coating Conditions

Control 1	PDL on glass (No glue)
Control 2	PDL+Laminin on glass (No glue)
Condition 1	PDL on PDMS
Condition 2	PDL+Laminin on PDMS
Condition 3	30 secs Plasma+PDL+Laminin on PDMS
Condition 4	2 min Plasma+PDL+Laminin on PDMS
Condition 5	2 min Plasma+PDL on PDMS
Condition 6	PDL+Laminin Coating by Desiccation

Table 2.1: Table of initial coating conditions tested.

Control 1	PDL on glass (No glue)
Control 2	PDL+Laminin on glass (No glue)
Control 3	PDMS only
Condition 1	PDL on PDMS
Condition 2	PDL+Laminin on PDMS
Condition 3	30 secs Plasma+PDL on PDMS
Condition 4	30 secs Plasma+PDL+Laminin on PDMS
Condition 5	PDL+Laminin Coating by Dessication

Table 2.2: Table of coating conditions tested.

The details of the coating procedures for each condition are given below.

O₂ Plasma

In order to tune the hydrophilicity of the PDMS surface, oxygen plasma cleaning was performed using the plasma cleaner PDC-32G (Harrick Plasma, Ithaca, NY, USA) where the PDMS substrate was exposed to 2×10^2 mbar pressure using high power for 30 seconds and 2 minutes depending on the experimental group.

PDL Coating

PDL coating solution was prepared by adding 1 mL of PDL (P7280, Sigma-Aldrich) stock was thawed and mixed with 8 mL of sterile PBS (10010015, Gibco, Thermo Fisher Scientific, Switzerland). 2 mL of the PDL solution was added to each dish and incubated at 4 °C over night. The

PDL solution was washed 3x with PBS and then once 1x with sterile DI water. PDL solution should be washed completely since non-physisorbed PDL polymer fragments can be toxic for the neurons. [?] [?]) Finally, the dishes were dried in the hood for 1 hr.

Laminin Coating

In order to prepare the laminin coating solution of concentration 10 $\mu\text{g}/\text{mL}$, 50 μL laminin (1 mg/mL) stock was thawed on ice to prevent gelation and was later added to 5 mL NeurobasalTM plus medium (A3582901, Gibco). For experimental groups involving laminin coating, the surface of dish was covered 2 mL with the laminin solution after the PDL washes and incubated over night at 37 °C incubator or at 4 °C for 48 hours. After the incubation, laminin solution was washed 1x with PBS and 2x with sterile DI water to avoid formation of salt crystals.

Coating by Desiccation

Firstly, structures were mounted and glued to a small Petri dish coated with PDMS and cured at 80 °C for 2 hours as described in Section 2.4. After the curing, PDL was added directly (3 mL) and desiccated for 30 mins. After the channels have been filled, PDL was incubated for 1 hr at RT followed by X3 PBS washes with 10 minutes waiting in between every wash. Finally, a X1 wash with sterile water was performed, laminin (3 mL) was added and incubated overnight in the incubator. The next day, laminin was washed with X1 PBS and X3 with sterile DI water with 10 minutes of waiting in between each wash step.

2.4 Microstructure Gluing and Mounting

Prior to mounting, any small particles that might cause dust contamination or leakage was removed by using scotch tapes. [?] After the last PDL or laminin wash with sterile DI water, micro-structures were mounted immediately to minimise drying of laminin. A drop of sterile water was used to mount structures on the glass. 3-well 4 um or 6 um structures were cut and transferred to the glass dish and gently sealed off to the bottom. Once the mounting was completed, as much DI water was removed as possible and then the dish was transferred to the 40 °C oven. The mounted structures were dried for 1 hr. For the experimental groups, the structures were glued on the PDMS coated petri dishes as described previously in Section 2.2.2, using a PDMS:Hexane dilution ratio of 1:40 and cured in the oven at 80 °C for 2 hours. Once all the structures were mounted and dried or cured, PBS was added to the dishes and the dishes were desiccated in dessicator chamber for 30 mins to ensure the filling of the channels. After desiccation, the micro-channels were examined under the microscope to confirm filling of the channels and presence of no bubbles. Desiccation procedure was repeated if the channels were not completely filled or bubbles were observed in the micro-channels or the output channel. Once the channels were filled, PBS was replaced with RGC for retina explants and Neurobasal Plus medium supplemented with B27+ and anti-anti for cortical spheroids before seeding cells.

2.5 Coatings Troubleshooting Experiment

Combination of potential factors such as heat treatment, uncured PDMS and plasma treatment that might have a detrimental effect on the coating were tested systematically using the 4 μm 3-well structures without glue. After curing PDMS, residual uncrosslinked oligomers can remain in the polymer network which might leak into the micro-channel medium or affect the wetting dynamics. These oligomers can be extracted by using a solvent such as toluene in order to swell the bulk PDMS. [?] [?] The combinations tested are given in Table ??.

Control	PDL+Laminin on Glass
Condition 1	Toluene Wash+Plasma+PDL&Laminin+Heat 80°C
Condition 2	Toluene Wash+No Plasma+PDL&Laminin+Heat 80°C
Condition 3	Toluene Wash+Plasma+PDL&Laminin+No Heat
Condition 4	Toluene Wash+No Plasma+PDL&Laminin+No Heat
Condition 5	No Toluene Wash+Plasma+PDL&Laminin+No Heat
Condition 6	No Toluene Wash+No Plasma+PDL&Laminin+No Heat

Table 2.3: Table of coating conditions tested.

Two PDMS substrates were prepared from the same batch by spin coating two different glass wafers (3 inches) at 500 rpm for 60 secs (not so thin to make it easier to cut) and cured at 80 °C for 2 hours. One of the PDMS substrates was used for the groups with no toluene wash whereas the other one was washed with toluene adapting the protocol by Monier et al. [?]. The structures and PDMS substrate for the toluene wash groups were soaked in a toluene bath filled with 40 mL of toluene for 24 h hours where the toluene was replaced twice during the day. The substrate was later de-swelled in ethanol (100 %) for another day where the ethanol was also replaced twice. During de-swelling, the PDMS substrates should be aligned back on the glass wafer. Finally washed structures and substrate were placed in a vacuum oven at 80 °C for 5 hours. Once the substrates were ready, rectangular pieces were cut and mounted on the substrates and the respective treatment was applied according to the group condition. Plasma or no plasma treatment was followed by PDL and laminin coating. Finally structures were mounted on substrates and they were dried in the 40 °C oven for 1 hour for no heat condition and at 80 °C for 2 hours for heat conditions.

2.6 Coating Uniformity after Desiccation

In order to check the uniformity of the coating of the microchannels and the output channel by desiccation, fluorescent PDL was used. PDL was rendered fluorescent using atto 425-NHS fluorophore (Sigma-Aldrich). Firstly, 1 mL of 0.5mg/mL PDL was thawed, 50 μL of atto 425-NHS was added and the solution was vortexed and incubated at room temperature for 1 hour protected

from light by an aluminum foil cover. After the incubation, PDL was diluted to final concentration with PBS. Fluorescent PDL was later added to a dish with structures mounted and the dish was desiccated for 30 mins. The dish was incubated at 4 °C overnight and imaging was performed the next day using CLSM with an excitation at 445 nm.

2.7 Primary Cell Culture

All cell culture experiments were performed using primary cells from cortices and eyeballs of E18 embryos of time-mated pregnant rats (Janvier Laboratories, France). Animal experiments were approved by the Cantonal Veterinary Office Zurich.

2.7.1 Retina Dissections

Dissection instruments, microscalpels, scissors and forceps were sprayed with 70 % ethanol prior to dissections. The retina dissections were performed under a benchtop microscope (DFC420C with 4X magnification, Leica, Germany) in a Petri dish filled with hibernate medium. Retinas were dissected out from whole eyeball. Firstly, all the tissue around the eyeballs was removed. The eyeballs were pinched along the cornea-sclera edge and cornea with forceps on both sides and gently pulled apart to cut open and isolate the retina. After gently removing the lens, the retina was later cut into square explants of around size 500 μm X 500 μm . After the dissections, the 100 μL dissected retina explants were transferred to a small Eppendorf tube and tagged with an adeno-associated virus (AVV) encoding for the mRuby virus (scAAV-DJ/2-hSyn1-chl-mRuby3-SV40p(A)). To do so, mRuby virus vial was thawed on ice and 1 μL was added to the explants. The explants were incubated with mRuby on ice for 1 hour.

2.7.2 AggreWell™ Preparation and Cell Dissociation

AggreWell™ plate preparations to produce reproducible spheroids and cell dissociation were performed in parallel. AggreWell™ 800 microwell culture plates were prepared by adding 500 μL of AggreWell™ rinsing solution to the needed wells in order to prevent cell adhesion and promote spheroid formation. The plate was then balanced by adding 300 μL of DI water to each well of a standard well plate and centrifuged at 2000 x g for 5 minutes. The plate was examined under the microscope and check for bubbles. If there are trapped bubbles in the micro-well, the centrifuge procedure was repeated again. Afterwards, the AggreWell™ rinsing solution was aspirated and each well was rinsed with 2 mL of warm Neurobasal medium. 1 mL of complete medium was added to each well and the plate was kept in the incubator until cell dissociation was completed. For the cell dissociation, firstly, PBG solution was prepared by mixing 50 mg BSA in 50 ml sterile PBS together with 90.08 mg glucose. In order to prepare the Papain solution, 2.5 mg Papain was added to 5 mL of PBG and vortexed. After allowing 30 mins for dissolving, the solution was sterile filtered using a 0.2 μm filter. Finally, 5 μl DNase was added. 5 ml Papain solution was added, mixed gently and incubated at 37 °C for 15min and was shaken gently every 5min. Papain solution

was aspirated without disturbing the pellet and 5ml Neurobasal media supplemented with 10 % FBS was added. After waiting for 3 min, media was removed without disturbing the pellet. This wash step was repeated twice by adding 5 ml Neurobasal media, waiting 3 minutes and removing medium. Finally, 4mL Neurobasal Plus medium supplemented with B27+ and anti-anti was added for 8 cortices. The cortices were then pipetted up with a 5 mL Pipette boy and quickly ejected to dissociate the cells. The cells were strained using a 40 μm cell strainer and a cell count was performed using Trypan Blue and a hemocytometer. Once the viable cell concentration was determined, concentration of the cell suspension was adjusted to determine the number of cells required to obtain 8000 cells per microwell based on the desired number of cells per microwell multiplied by 300 microwells per well. After adding the required volume of the cell suspension to the wells, complete medium was added to each well to have a final volume of 2 mL in each well. 1 μL mRuby and with 0.5 μL of the calcium indicator was added into each well(s) to transduce the cells. The medium in the wells were pipetted up and down to make sure cells were evenly distributed. AggreWell™ plate was balanced again and immediately centrifuged at 100 x g for 3 minutes to ensure that the cells were captured in the micro-wells. Even distribution of cells inside the micro-wells were confirmed under the microscope and the plate was incubated at 37 °C with 5% CO₂ for 24 hours before seeding to allow for the formation of spheroids.

2.8 Stretchable Microelectrode Arrays

2.8.1 Fabrication

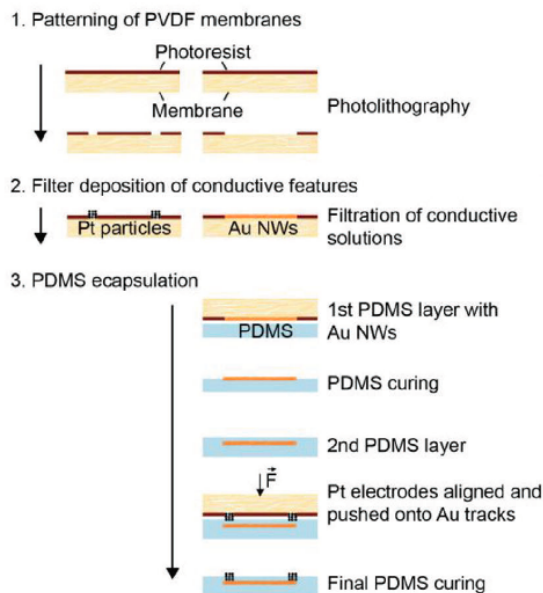


Figure 2.4: Fabrication steps of stretchable electrodes on a PDMS substrate with gold nanowire (Au NW) tracks with platinum (Pt) electrodes. [?]

The fabrication of the stretchable electrodes on a PDMS substrate with gold nanowire (Au NW) tracks with platinium (Pt) electrodes was based on Renz. et al [?]. Firstly, polyvinylidene fluoride (PVDF) filter membranes were patterned using photolithography in order to create masks for both the Au NW tracks and Pt particle electrodes. In the second step, Au NWs or Pt particles in distilled water were filter deposited through the respective mask. In the final step, the deposited Au NW tracks were embedded in semi-cured PDMS and Pt particles were aligned on top of a second PDMS layer and brought in contact with the Au NW tracks. The process is summarised in Figure 2.4. Stretch MEA was then transferred to a square glass or PMMA substrate that fits into the multichannel system (MCS). The design was adapted in order for the pads to fit.

2.8.2 Microstructure Alignment and Mounting on (MEA) Electrodes

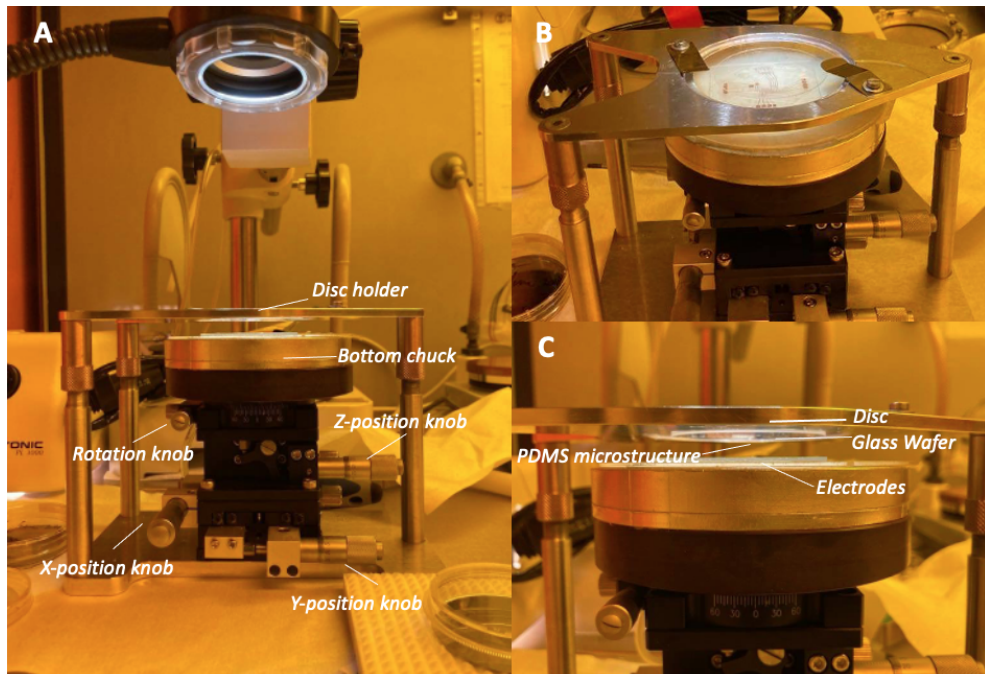


Figure 2.5: The custom made alignment set-up based on a stage with controls in x,y,z and theta. (A) Image of the complete set-up with all the components. (B) Top-view of the set-up. (C) Side-view of the set-up.

Mounting of the structures using the glue should be done in one go in order to prevent the clogging of the channels which is a challenge while aligning the structures at a specific location on the electrodes. Precise alignment is crucial since misalignment can lead to leakage, escaping of axons and inadvertent stimulation. For precise alignment of the PDMS micro-structures and proper sealing and bonding on electrodes using the glue, a custom made alignment set-up based on a stage with controls in x,y,z and theta was used for the alignment and gluing procedure. The set-up shown in Figure 2.3 consists of a disc holder at the top where the silanised glass wafer was attached to the disc via capillary forces by adding a drop of water and gently pressing it on the

disc. This way, the structures can be attached to the glass wafer during the alignment procedure. It should be noted that the glass wafer must be silanised otherwise bonding of the structure to the glass will be stronger and structure is likely to stay attached to the glass wafer rather than PDMS electrode surface which might result in the glue being smeared around. The structure was placed at the top where the transparency of the PDMS allows precise alignment since the electrode tracks will be clearly visible below the microstructures in the upright set-up. Also it is critical that the disc holder stage is angled to be able to seal of the structure without any bubble formation. The electrode was placed on the lower chuck and held in place via vacuum.

A PDMS:Hexane glue concentration of 1:40 was prepared and spin coated on a clean silicon wafer as previously described. The disc and glass wafer assembly was removed from the upper chuck and placed on the bench. The structure was later stamped on the thin membrane of glue on the wafer with channel side with microfluidic features facing down and later was placed on the centre of the glass wafer with the glued channel side facing up and the corners of the structure were gently pressed down to ensure sealing and prevent hanging edges. Finally, the ring was placed back on the upper chuck of the mask aligner with the glued side of the structure with microfluidic features facing down on the electrode. Alignment was performed by adjusting the rotation angle and correcting the X and Y positions using the mask aligner knobs. Once the right alignment configuration was achieved, the chuck was moved up until the full contact, sealing off of the PDMS micro-structure and the electrode surface. The chuck was then carefully moved down leaving the micro-structure glued on top of the electrode tracks. This step should be done slowly in case one corner of the structure remains attached to the glass wafer to allow enough time to fall and seal. The electrode-micro structure assembly was cured at 80 °C overnight with 2 g weight on top to in order to ensure sealing and filling of the uneven gaps with glue.

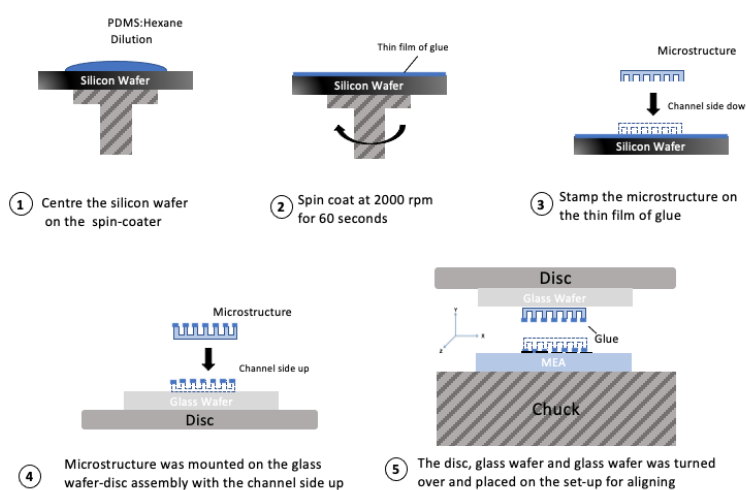


Figure 2.6: Schematic illustration of the steps involved in the alignment and gluing procedure.

2.8.3 Mounting PDMS rings and coating of electrodes

After the alignment and gluing of the structure, prior to coating the electrodes with PDL and laminin, PDMS rings with a 5 mm height and same diameter dimensions as the standard glass ring option of MEAs (inner diameter(ID): 19 mm, outer diameter (OD): 24 mm, Multichannel systems) were fabricated in order to create a reservoir. To fabricate the rings, PDMS substrate was prepared as previously described and poured into a big Petri dish to obtain a height of around 5mm. Scribe-compasses was used to accurately mark 19 mm and 24 mm inner and outer diameters on the PDMS and a scalpel was used to cut out the rings. In order to glue the rings on the MEAs, PDMS was spincoated on a glass wafer at 500 rpm for 60 secs. The PDMS rings were stamped on spin-coated PDMS and placed around the microstructureounted on the stretch MEA. PDMS was added round the edges of the outer and inner diameters to fill in any remaining gaps and ensure a good seal using a syringe needle(1.2x40mm, BD Microlance (TM) 3). Finally, the complete assembly was cured at 80 °C for 2 hours. For the coating procedure, 1 mL PDL solution was added into the reservoir on the electrodes and the dish was dessicated for 30 mins to force PDL into the microchannels. MEAs were incubated with PDL at room temperature for 1 hour followed by X3 PBS washes and X1 sterile DI water wash while waiting for 10 minutes in between every wash step to allow enough time for the micro-channels to be completely washed. Finally, 1 mL laminin solution was added, dessicated for 30 mins and incubated overnight at 37 °C with 5% CO₂. Before cell seeding, the reservoir was washed X1 with PBS and X3 with sterile DI water. Finally, for cortical spheroids, 1 mL Neurobasal plus medium supplemented with B27+ and anti-anti was added to the reservoir. As a coating control, structures were also mounted on photo-resist and glass.

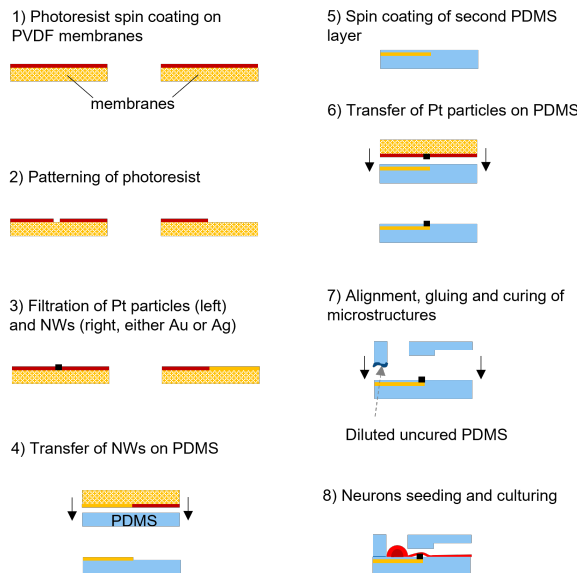


Figure 2.7: Summary of the fabrication and gluing process for the microstructure-MEA assembly.

2.9 Cell Seeding and Primary Neuronal Cell Culture

Explant and spheroid seeding into the wells were performed under a benchtop microscope (DFC420C with 4X magnification, Leica, Germany). Virus tagged explants and spheroids were gently pipetted and transferred to the wells of the mounted structures. Microscalpels were later used to insert the explants or spheroids into the wells. After the seeding, a small petri dish (\varnothing 40 mm) was filled with 2 mL of sterile DI water supplemented with 5 % anti-anti and placed next to the culture dish in the big dish in order to minimise evaporation of the cell culture medium and prevent drying out of the structures. For the electrodes, a cover was placed on top of the PDMS ring. Finally, cell culture dishes were transferred to the incubator and kept undisturbed for 3 days at 37 °C , 5 % CO₂. A half-medium change was performed every 2 days by using RGC medium for retina explants and Neurobasal plus medium supplemented with B27+ and anti-anti for cortical spheroids.

2.10 Image Acquisition

Confocal images were acquired using the inverted FLUOVIEW FV3000 confocal laser scanning microscope (CLSM), at DIV4, 7, 15, 22 and 30 using the X10 lens with a resolution of 1024X1024 (pixel size 1.24 μm). A grid scan of 3 by 6 was used to capture the whole micro-structure. mRuby was excited at 561 nm and the emission peak was detected in the red channel around 630 nm. A fiberglass incubator chamber was placed around the microscope to keep the temperature and CO₂ constant at 37 °C with 5% respectively. Images of the axonal growth on the electrode pads and tracks was acquired using the upright LSM 780 CLSM (Carl Zeiss, Switzerland) with the X5 lens (Fluor 5x/0.25 M27) and a resolution of 1400 X 1400 (1.21 μm). A tile scan of 5 by 2 was used to capture the growth inside the microchannels and on the tracks. mRuby was again excited at 561 nm and the emission peak was detected in the red channel. A heated well-plate holder and a plastic incubator box was used to keep the temperature and CO₂ constant at physiological values. The cells were transported using inkigo.

2.11 Image Analysis

Parameters used to evaluate the coating's ability to enhance axonal growth and cell adhesion were % filled channels, % surface area covered by axonal growth, distance travelled by the axons in the output channel and bundling inside the output channel. Image analysis was performed using Python and ImageJ. The acquired images were separated into channels and a log transform ($S = \text{clog}(r+1)$ or $f(p) = \log(p) * 255/\log(255)$ to each pixel (p)) was applied to the red channel images for image enhancement using ImageJ. Red channel images were saved as 8-bit and imported to the Python script. For the pre-processing step, the images were firstly converted to grayscale and later median filtered with a kernel size of 3X3 to get rid of the background salt and pepper noise. Otsu thresholding was used to binarize the images and morphological operations, namely, closing and dilation were performed to achieve uniformity and to get rid of microchannels to be able to quantify

the explant area only by contour detection. During the post-processing step, % filled channels, % surface area covered by the axons and distance travelled in the output channel were evaluated to quantify axonal growth within the microstructures in each coating condition. Furthermore, the mode of axonal propagation in the output channel was analysed based on bundling. The number of axon filled channels were quantified by plotting the intensity profile of a rectangular section along the microchannels in x-direction and automatically detecting the number of the peaks that correspond to the number of open filled channels. The values were given as a percentage value as given in Equation 2.1:

$$(\%) \text{ Filled Channels} = \frac{\text{Counted Peaks}}{\text{Total No. of Microchannels in the microstructure (60)}} \times 100\% \quad (2.1)$$

In order to quantify, % surface area covered by the axonal growth, pixels in the binary image were counted and multiplied by 1.24^2 , based on resolution, to obtain the total area including explant and channel area covered by the axonal growth in μm^2 . Due to the non-uniform size and shape of the explants which might influence the results, only the % axonal growth in the channels was quantified as the total area of the explants subtracted from the total area of the quantified growth area similar to the method described by [?]. The growth area covered by axonal growth was given as a percentage as given in Equation 2.2:

$$\text{Growth Area (\%)} = \frac{\text{Growth Area (excluding explants)}}{\text{Total channel area of the microstructure (excluding wells)}} \times 100\% \quad (2.2)$$

In order to quantify the distance travelled by the axons in the output channel, the intensity profile of a rectangular segment along the output channel in y-direction was plotted. The profile was smoothed using a 5x5 low pass filter to get rid of the noise to better detect peaks and distance in pixels was calculated by taking the index of max and min points from the intensity profile. The pixel measurements were later converted to microns (multiply by 1.24). Finally, to quantify the "mode of growth" along the output channel, 10 segments were taken along the output channel and intensity profile of each individual segment in x-direction was fitted to a Gaussian distribution defined by Equation 2.3.

$$f(x) = ae^{-\frac{(x-\mu)^2}{2\sigma^2}} \quad (2.3)$$

where a is the amplitude, μ is the position of the centre of the peak and σ is the standard deviation. Bundling ratio was later quantified as the ratio between the amplitude of the fitted peak and sigma which represents the width of the bundle. For growth that occupies all the width of the output channel, the peak will have a low value and the sigma will have a high value leading to a ratio of lower than 1. On the other hand, a bundle will result in a value higher than 1 due to a higher peak value and a lower sigma value. The summary of the image processing pipeline is given in Figure 2.5.

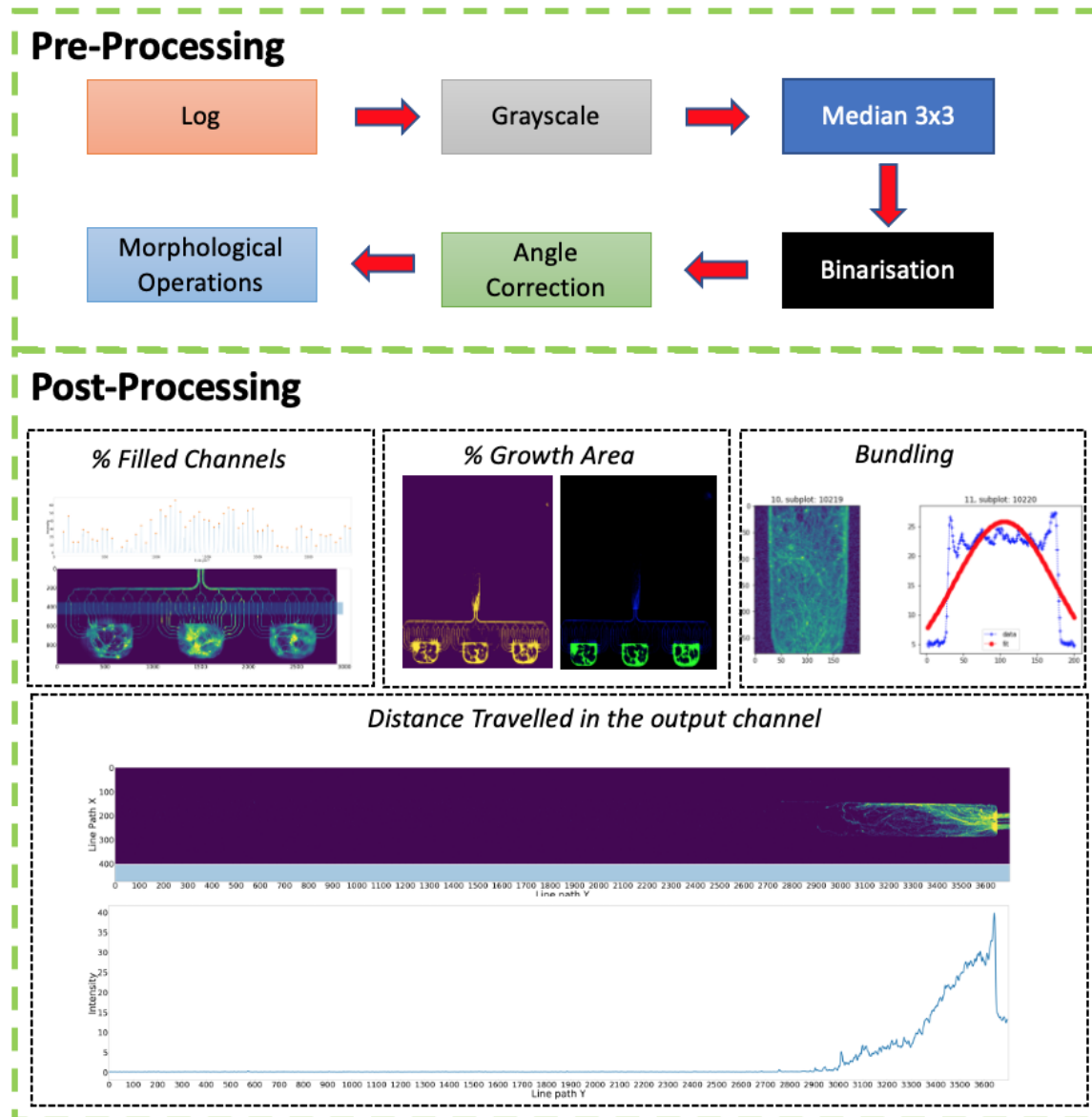


Figure 2.8: Summary of the image processing pipeline.

2.12 Statistical Analysis

All the coating experiments were performed with triplicates ($N=3$) and different coating groups were compared at the same time points using a one-way ANOVA for multiple comparisons (Kruskal-Wallis). p value of less than 0.05 was considered as statistically significant. For the bundling analysis, the bundling ratios were also compared at the same days within different groups using a one-way ANOVA. All the statistical analyses were performed using GraphPad Prism 6 software package (GraphPad Software, Inc., San Diego, CA, USA).

2.13 Re-using the microstructure-electrodes assembly

The protocol to clean and re-use the electrodes was adapted from the procedure described by Wheeler et al. [?]. Firstly, the medium was pipetted up and down using the 1000 pipette in order to resuspend the spheroids or explants out of the wells. The medium was later aspirated and 1 mL of 1 % Tergazyme (Z273287, Sigma-Aldrich) was added for 2 hr where 1 % Tergazyme was replaced twice and left to incubate at room temperature overnight. In order to force any remaining cell debris out of the output channel and wells, the dishes were dessicated for 30 mins and sonicated for 15 minutes. The structures were visually inspected under the microscope to confirm that all the visible cell debris was removed. After the overnight incubation, 1 % Tergazyme was removed and structures were washed X3 with sterile DI water with 10 minutes wait in between every wash step. Next, 70 % ethanol was added for 40 minutes and then washed X3 with sterile DI water with 10 minutes waiting between every wash. The structures were left in sterile DI water overnight to completely wash ethanol.

2.14 RGC Growth Medium Preparation

Neurobasal Plus (Gibco, A3582901)	237.5 mL	4°C
DMEM (Gibco 11960)	237.5 mL	4°C
Glutamax	5 mL	4°C
Sodium Pyruvate (100mM, Gibco 11360-070)	5 mL	4°C
Antibiotic-Antimycotic (100x, Gibco 15240096)	5 mL	-20°C
N2 Supplement	5 mL	-20°C
B27+ (50x)	10 mL	-20°C
N21 Supplement (50x, R&D Systems AR008)	10 mL	-20°C
NAC Stock (5 mg/mL) (reduces apoptosis)	500 µL	-20°C
Forskolin Stock (4.2 mg/mL)	500 µL	-20°C
BDNF Stock (50 µg/mL, Preprotech 450-02)	500 µL	-20°C
CNTF Stock (10 µg/mL, Preprotech 450-13)	500 µL	-80°C
NGF 7S Stock (10 µg/mL, final 10 ng/mL)	500 µL	-80°C
GNDF (10 ng/mL)	500 µL	-20°C

Table 2.4: Table of all the components needed for the preparation of RGC medium.

Chapter 3

Results

3.1 PDMS:Hexane Glue

3.1.1 PDMS:Hexane Glue Dilution Ratio Optimisation

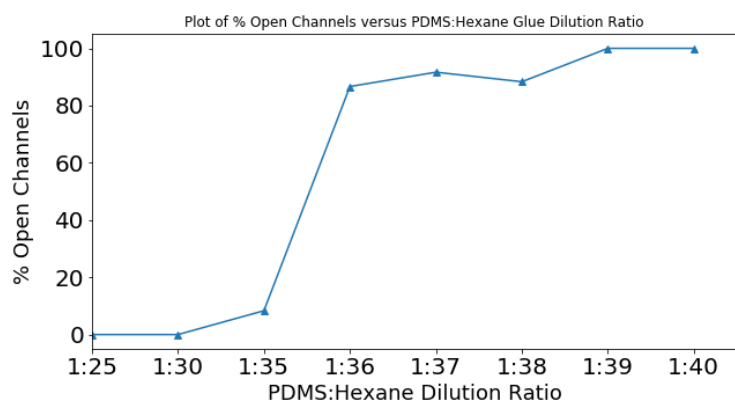


Figure 3.1: The graph of % Open Channels against varying PDMS:Hexane dilution ratios tested as glue for mounting the PDMS microstructures.

As depicted in Figure 3.1, most of the channels were clogged when the 1:25, 1:30 or 1:35 dilution ratios were used. Although there was a dramatic increase in the % open channels, after the dilution ratio 1:35, all the channels were open only for the glue dilution ratios of 1:39 and 1:40. The dilution ratios 1:39 and 1:40 were further tried on the transferred electrode surface which also showed that all channel were open. Moreover, the glue was cured after a week at room temperature and over several days at 40 °C whereas curing at 80 °C.

3.1.2 Reproducibility of the 1:40 dilution

	No. of Open Channels	No. of Clogged Junctions
Mean	58.95	1.40
Std	4.44	4.56

Table 3.1: Total number of open channels and total number of clogged junctions after the mounting procedure using 4 different batches of 1:40 PDMS:Hexane glue in 44 structures. ($N=44$)

As recorded in Table ??, 58.95 ± 1.40 of the microchannels were open whereas 4.44 ± 4.56 of the junction channels were clogged using the 1:40 PDMS:Hexane dilution ratio. Moreover, no axonal escape was observed in any of the 44 glued structures and axonal growth was successfully confined.

3.1.3 Bonding Strength of the 1:40 dilution

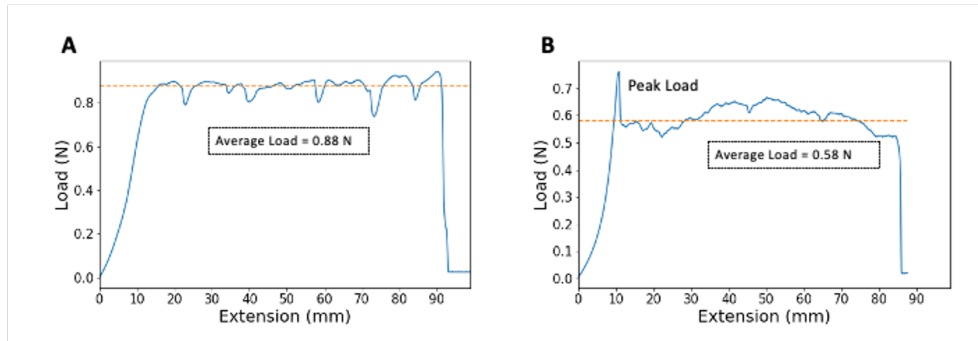


Figure 3.2: The results of the t-peel test using the tensile stretching machine. (A) Load-extension curve for the PDMS-PDMS bonded test specimens where the average peeling force is marked with the orange dashed line. (B) Load-extension curve for the 1:40 PDMS:Hexane glue bonded test specimens where the average peeling force is marked with the orange dashed line.

Figure ?? (A) and (B) show the typical load-extension curves for PDMS-PDMS and 1:40 PDMS:Hexane bondings. After the start of the test, the load begins to increase at a steady rate until reaching a maximum value, indicating that the specimen is taut, and remains around the same value during the peeling process as depicted in both Figures ?? (A) and (B). The dashed orange line in both graphs indicates the average peeling force during the t-peel test. The negative slope of the curve at the end indicates loss of stiffness thus debonding of the strips at the end of the test. Figure ?? compares the strain energy density among 1:40 PDMS:Hexane and PDMS glues as well as with plasma bonding where there were no significant differences observed between diluted and undiluted PDMS bonding. In addition there was a larger variability in the strain energy density of PDMS-PDMS and plasma bonded specimens compared to 1:40 PDMS:Hexane dilution glue.

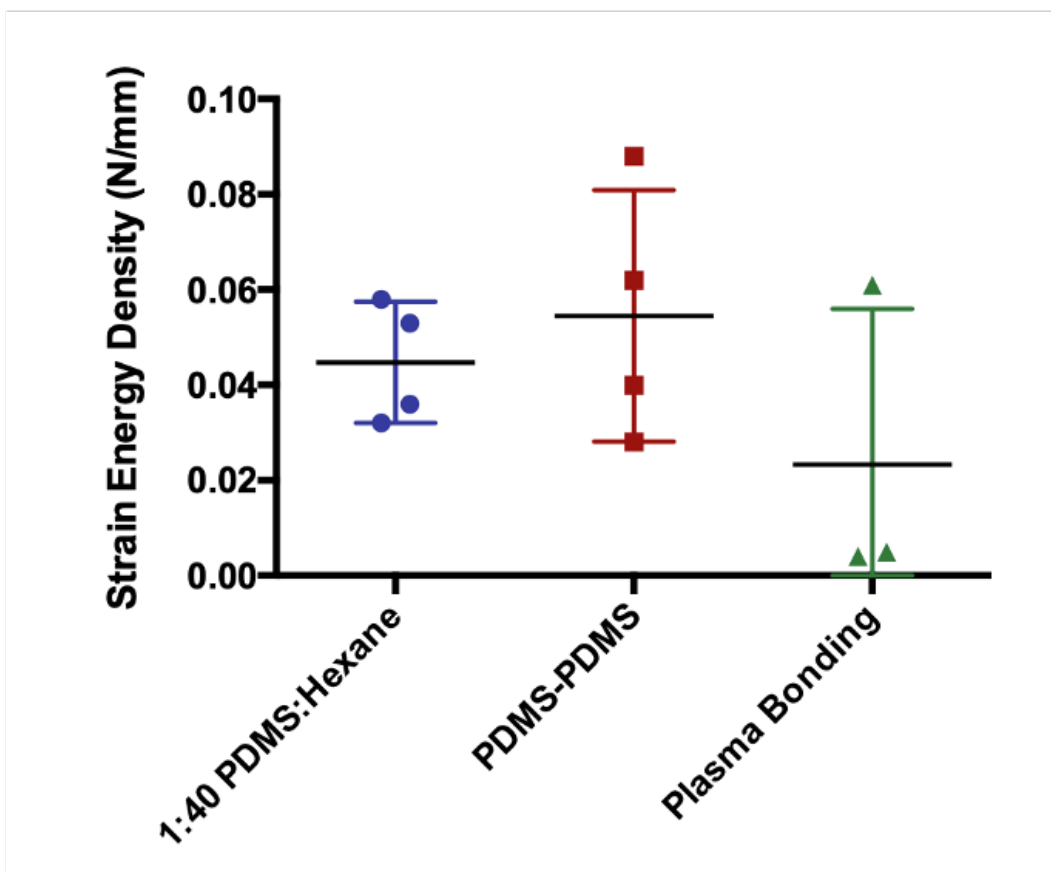


Figure 3.3: Graph comparing the strain energy density of the PDMS-PDMS glue, 1:40 glue and plasma bonding.

3.2 Coatings

As shown in Figure ?? (A), there are variations in the % channels filled with axons in different coating conditions where the axons grow inside the channels at different rates. The axons fill the most channels at the highest rate in the control group on glass coated with PDL+Laminin whereas PDL on PDMS shows only marginal filling of the channels over the course of 30 days. PDL+Laminin on PDMS and PDL+Laminin coating by Desiccation groups also follow a similar trend to the Control PDL+Laminin group with a slightly lower percentage of filled channels. The % filled channels start to decrease in the PDL+Laminin on PDMS group after DIV 7. Figure ?? (B) on the other hand shows that Control PDL+Laminin without heat treatment has the most significant % area coverage by the axons compared to the other groups. PDL+Laminin coating by Desiccation group shows the second most area coverage over the course of 30 days. Figure ?? (C) shows that Control PDL+Laminin and PDL+Laminin groups grow axons the furthest at the fastest rate in the output channel where they reach the end of the output channel (5 mm) by DIV 15. After DIV 15, the axon bundle in the PDL+Laminin on PDMS group collapses whereas the control PDL+Laminin group continues to facilitate axonal growth in the output channel.

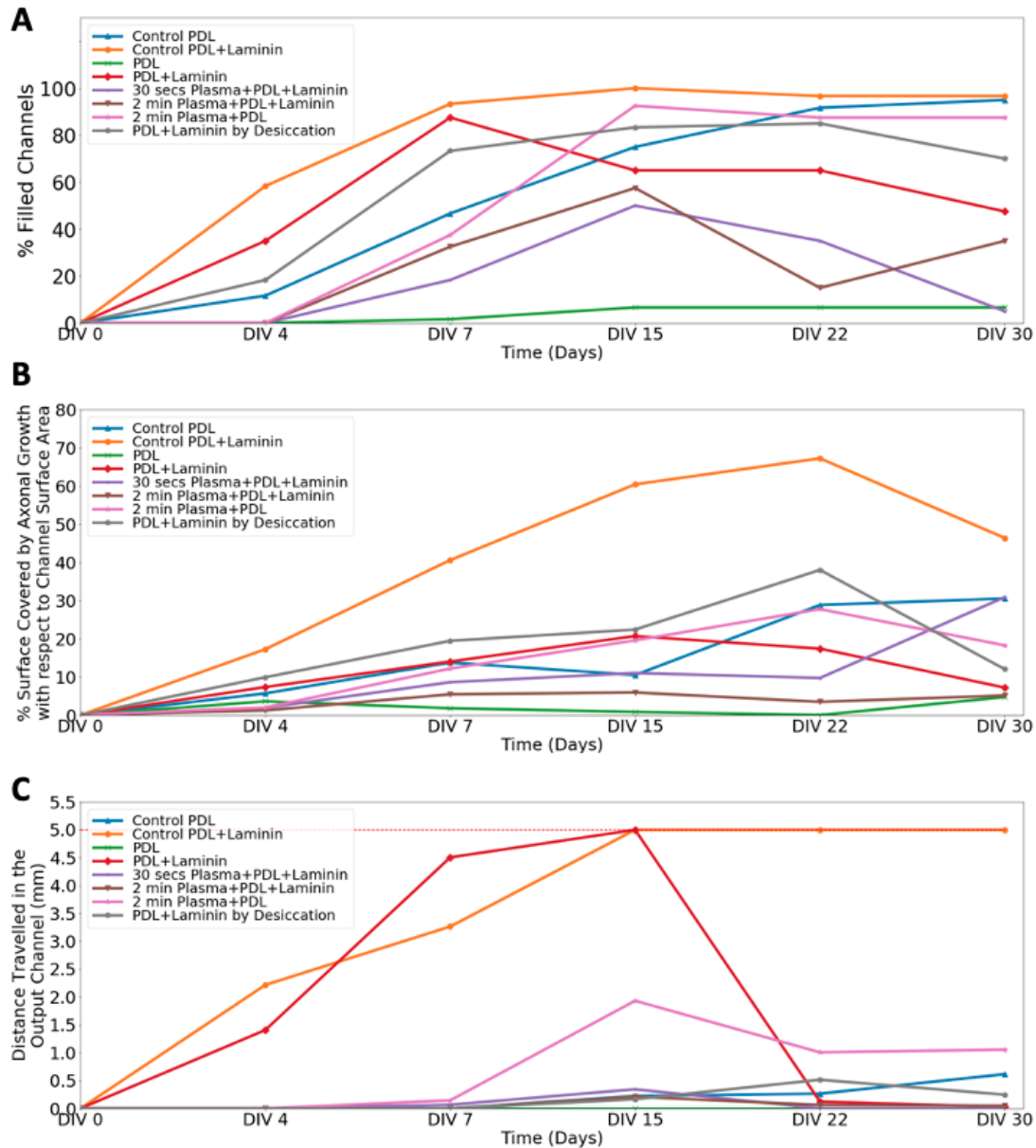


Figure 3.4: Graphs of different coating conditions tested to evaluate the nerve growth ($N=1$). (A) Graph showing % channels filled with axons for each coating condition over the course of 30 days. (B) Graph showing % surface area covered by axonal growth with respect to the total surface area of the microfluidic channels, excluding well and explant areas. (C) Graph showing the total distance travelled by the axons in the main output channel where the end of the channel is marked by a dashed red line at 5 mm.

As shown in Figure 3.5, Control PDL and laminin on glass and PDL+Laminin coating by Desiccation followed the same trend with the results from the previous experiment yielding consistent results. Moreover, the two groups were not significantly different from each other in terms of % filled channels and % surface area covered by the axonal growth. Distance travelled in the output channel was considerably higher in the control PDL and laminin group compared to all the other coatings. These results are consistent with the previous experiment, where the control PDL and laminin group was the gold standard in terms of axonal growth based on % filled channels, % surface area covered by the axons and the distance travelled by the axons in the output channel followed by the PDL+Laminin coating by Desiccation group. As depicted in ?? (A) At Day 4, the % filled channels are considerably more significant in Groups 4, 5 and 6 compared to the heat treat groups 1 and 2 as well as Group 3. Groups 1,2 and 3 followed a similar growth trend until Day 7 where the % filled channels increased at a slower rate compared to the other groups. Although all the channels were filled in Group 3 by the end of Day 22, heat treated groups Group 1 and Group 2 remained around 60 % and 40 % respectively. ?? (B) shows that the differences observed in % surface area covered by axonal growth in different groups were within the range of the error bars. The control group and Group 5 had a fast initial growth rate until Day 7 and remained dominant over the course of 30 days. As demonstrated in ?? (C), Groups 4, 5 and 6 as well as the control reached the end of the output channel by Day 7 where the growth rate in the output channel was the highest in Group 5. There was marginal increase in the axonal growth in the output channel in Groups 1 and 3 after DIV 7. After Day 22, axonal growth in the output channel in Groups 4 and 6 dropped back at Day 30 whereas axons continued to remain at the end of the output channel for Group 5 and Control PDL+Laminin.

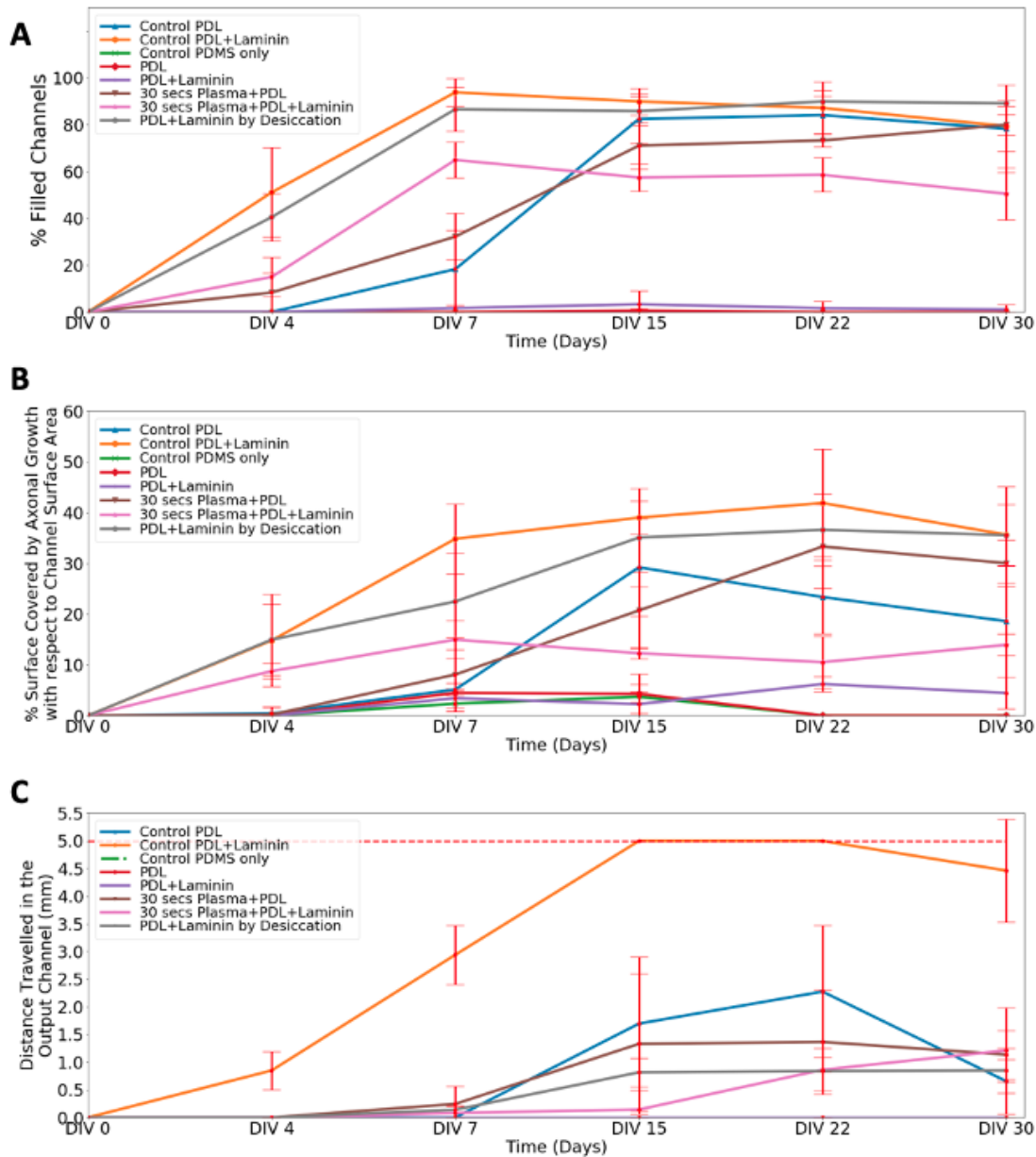


Figure 3.5: Graphs of different coating conditions tested to evaluate the nerve growth. ($N=3$). (A) Graph showing % channels filled with axons for each coating condition over the course of 30 days. (B) Graph showing % surface area covered by axonal growth with respect to the total surface area of the microfluidic channels, excluding well and explant areas. (C) Graph showing the total distance travelled by the axons in the main output channel where the end of the channel is marked by a dashed red line at 5 mm.

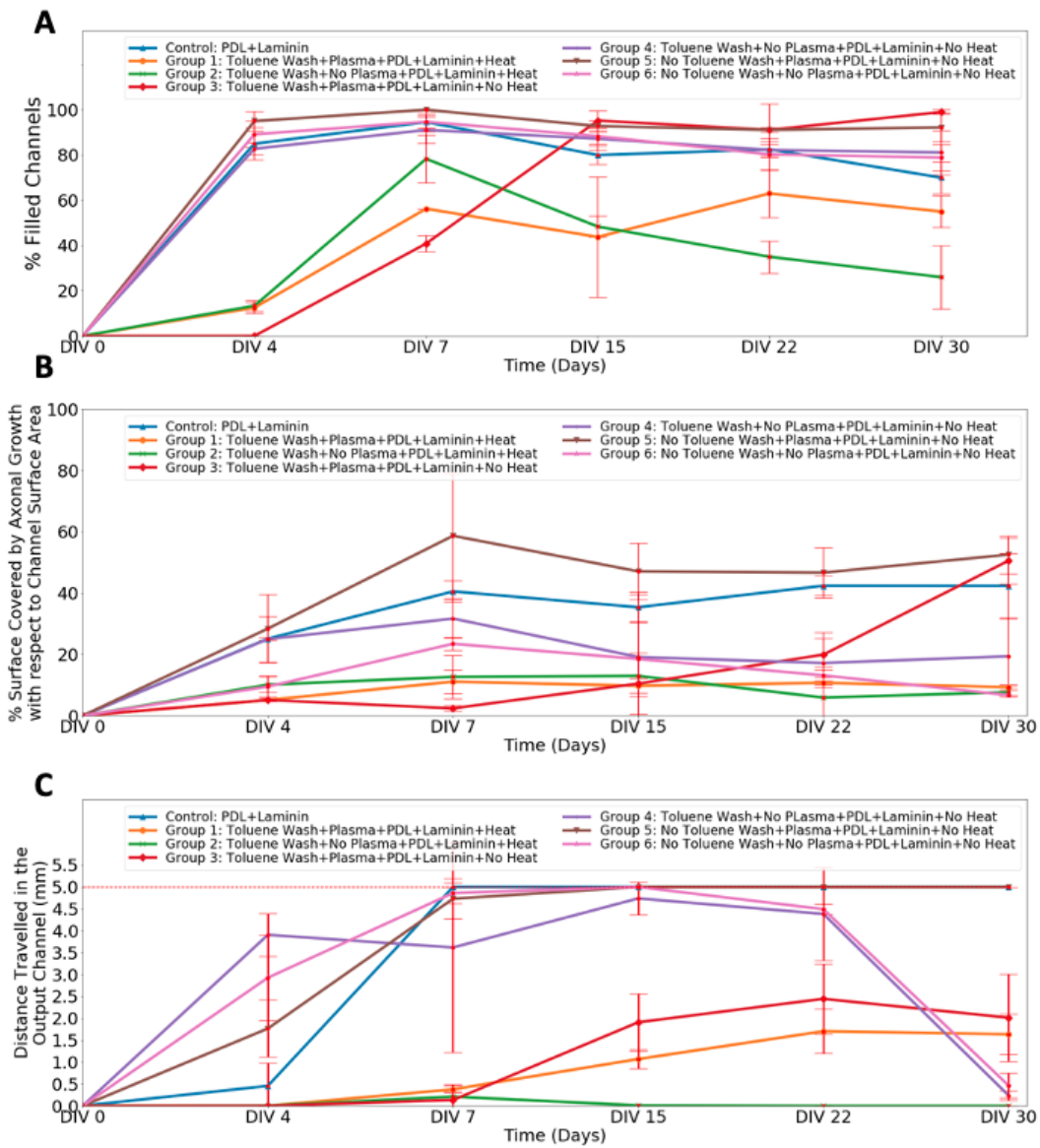


Figure 3.6: Graphs of different combinations of potential factors affecting the coating are tested ($N=3$). (A) Graph showing % channels filled with axons for each coating condition over the course of 30 days. (B) Graph showing % surface area covered by axonal growth with respect to the total surface area of the microfluidic channels, excluding well and explant areas. (C) Graph showing the total distance travelled by the axons in the main output channel where the end of the channel is marked by a dashed red line at 5 mm.

3.3 Bundling Analysis of Formation of Nerve Fascicles

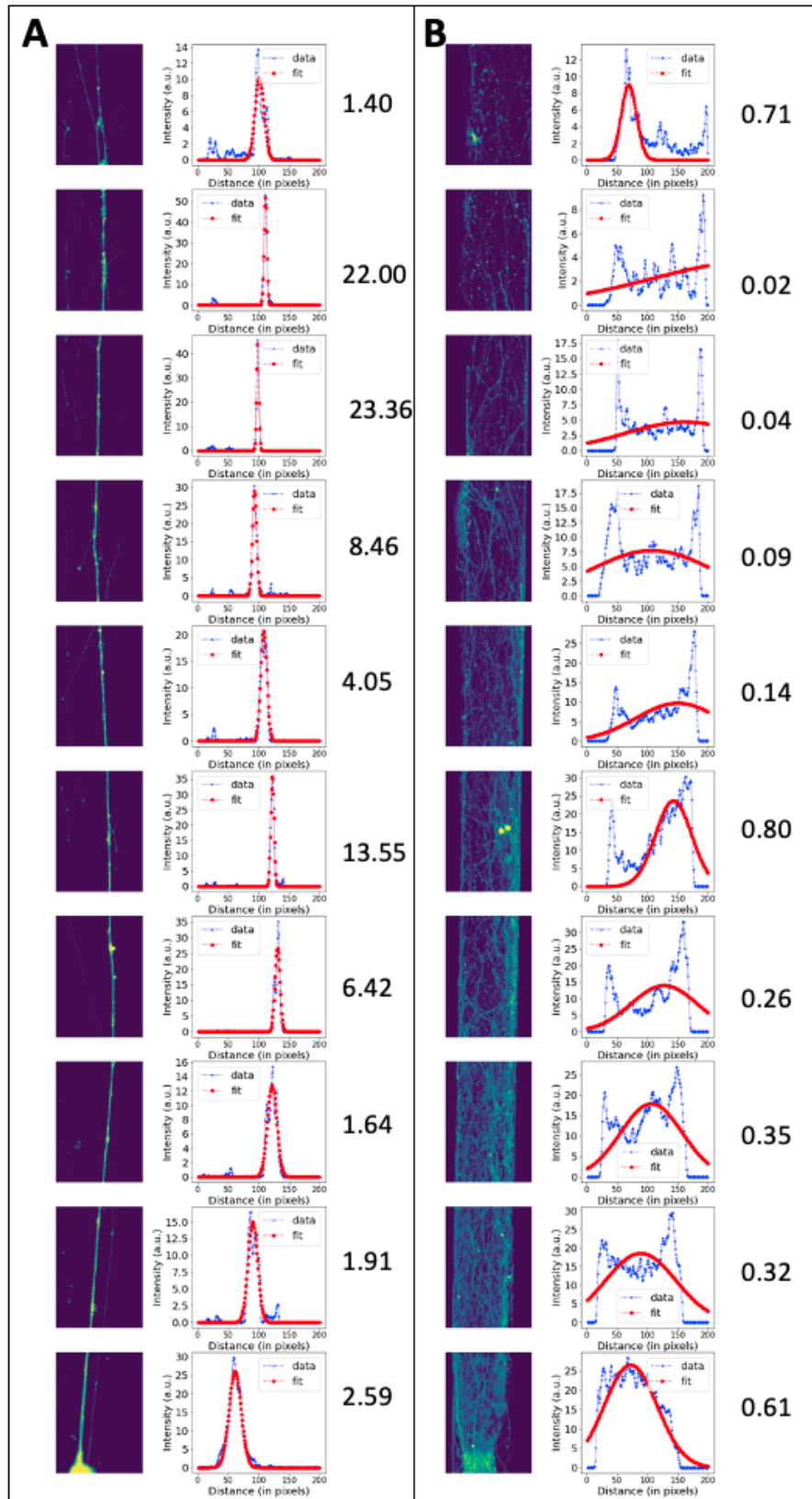


Figure 3.7: A representative bundling comparison between non-plasma coating condition where there is bundle (A) and non-plasma (B) coating condition with spread growth in the output channel.

Figure ?? shows 10 different segments taken along the output channel of each microstructure and the Gaussian fit for the intensity profile of each segment where the y-axis is the intensity and the x-axis is the distance in pixels. The Gaussian fit is indicated by the red line whereas the intensity profile is indicated by the red line. The values next to each segment represents the bundling ratio obtained. As depicted in Figure ??, the bundling in the non-plasma group yields bundling ratios of above 1 whereas Figure ?? shows the segments from the plasma-treated group where the axons grow in a more spread manner resulting in bundling ratios of below 1.

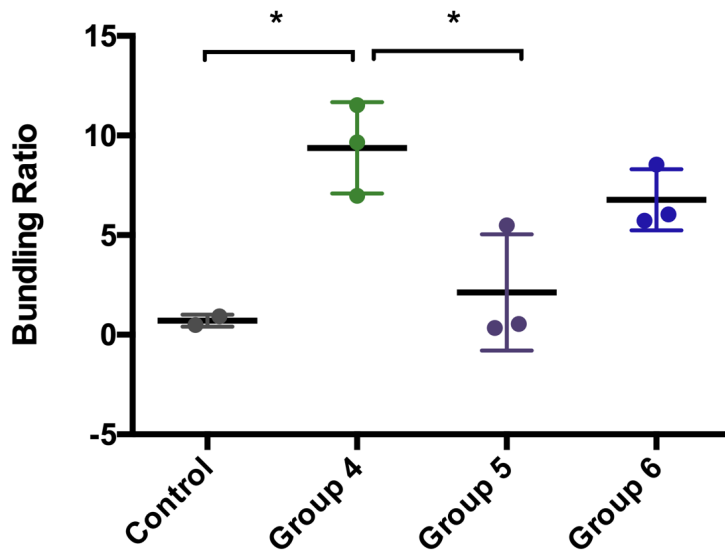


Figure 3.8: The graph of average bundling ratios along the 10 segments in the output channel for different groups at Day 15. Each marker represents the average of the bundling ratios along the output channel of a single structure. Higher bundling ratios indicate bundling whereas values close to 0 indicate spread growth. Control: PDL+Laminin coating on glass. Group 4: Toluene Wash+No Plasma+PDL and Laminin, No heat. Group 5: No Toluene Wash+Plasma+PDL and Laminin+No heat. Group 6: No Toluene Wash+No Plasma+PDL and Laminin+No heat.

Bundling analysis was performed at a time point where axons have reached the end of the output channel in majority of the groups at Day 15. Bundling ratios from double bundles were excluded. There was more bundling in the non-plasma treated groups Group 4 and 6, yielding a higher bundling index whereas bundling ratio was close to 0 for the plasma treated cases Group 5 and Control. There was a significant difference between Control and Group 4 whereas there were no significant differences observed between Control and Group 5 where both had no bundle. Furthermore, there was a significant difference between Group 4 and Group 5 whereas there were no significant differences observed between Groups 4 and 6 where both had bundle formation. As indicated by the box plot in Figure ?? and the values in Figure ??, only one case in Group 5 out of 3 formed a bundle leading to an increase in average bundling ratio along the segments.

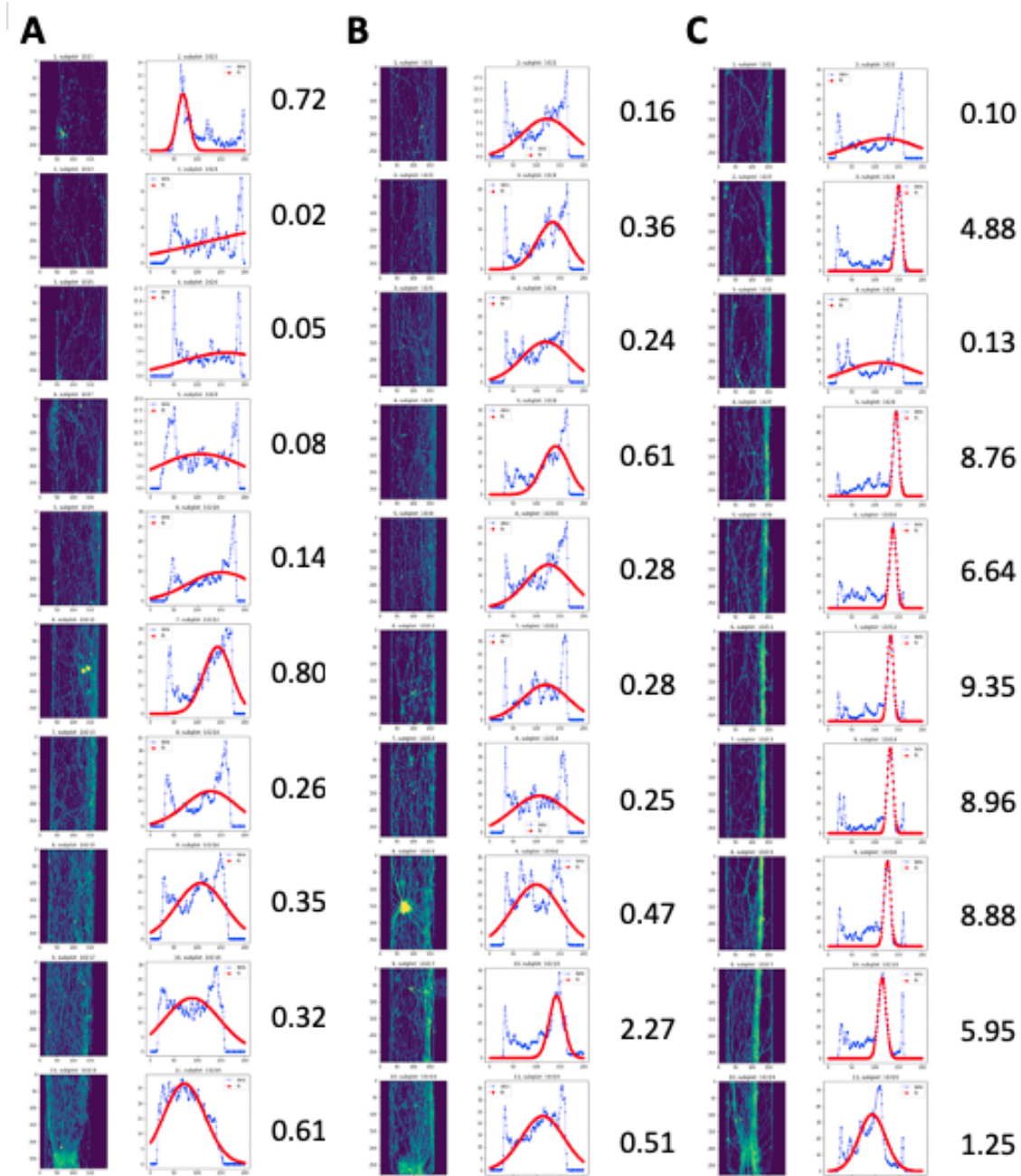


Figure 3.9: Segments from 10 different regions along the output channel of 3 plasma treated structures in plasma treated Group 5, Gaussian fit of the intensity profile of each segment and the bundling ratios corresponding to each individual segment of Structure 1 (A), Structure 2 (B) and Structure 3 (C) at Day 15.

3.4 Uniformity of Coating After Desiccation

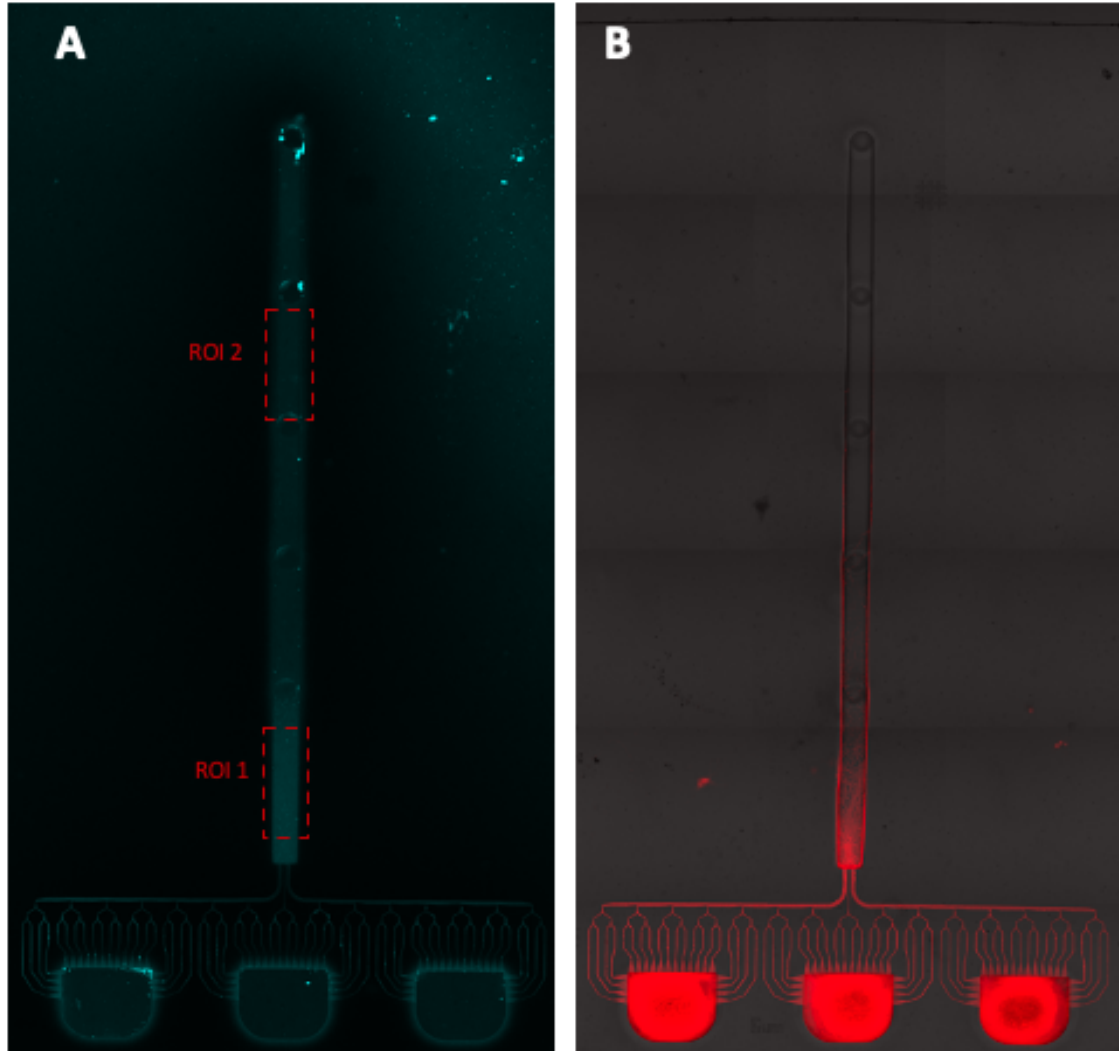


Figure 3.10: Coating and axonal growth inside the channels after coting by desiccation. (A) Fluorescent PDL inside the channels after coating by desiccation indicating two different ROIs analysed along the output channel. (B) Axonal growth inside the microchannels and along the output channel after PDL and Laminin coating by desiccation.

As shown in Figure ??, all the micro-channels were coated with fluorescent PDL uniformly. There was a difference observed in fluorescence between the beginning and end of the output channel where an intensity value of 49.93 in ROI 1 and 26.14 in ROI 2 was measured. The intensity value was higher in the beginning of the output channel in ROI 1 which is approximately the transition area where the distance travelled in the output channel by the axons reach and stop.

3.5 Electrode Alignments

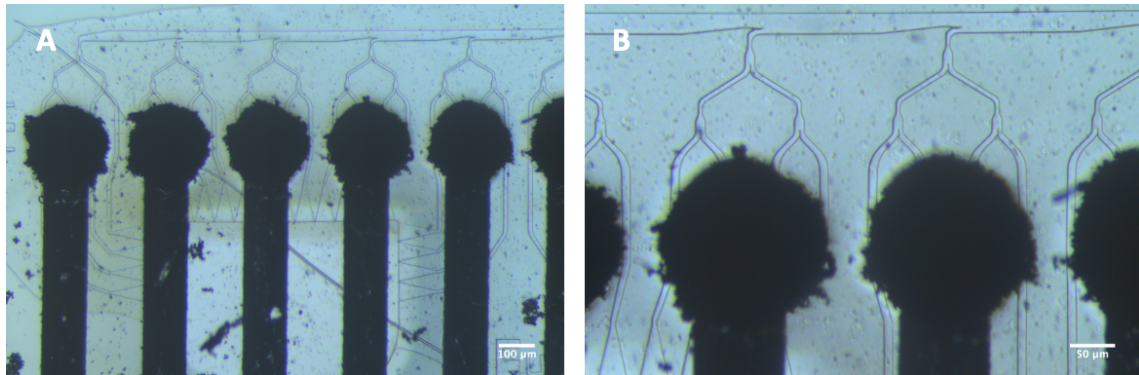


Figure 3.11: Images showing the micro-channels aligned with electrode pad and tracks with different magnifications using an inverted microscope. (A) Scale bar = 100 μm . (x10 Magnification) (B) Scale bar = 50 μm . (x20 Magnification)

Figure ?? shows that micro-channels of the PDMS microstructure were successfully aligned on top of the electrode track pads using the proposed alignment and gluing procedure.

3.6 Electrode Assembly

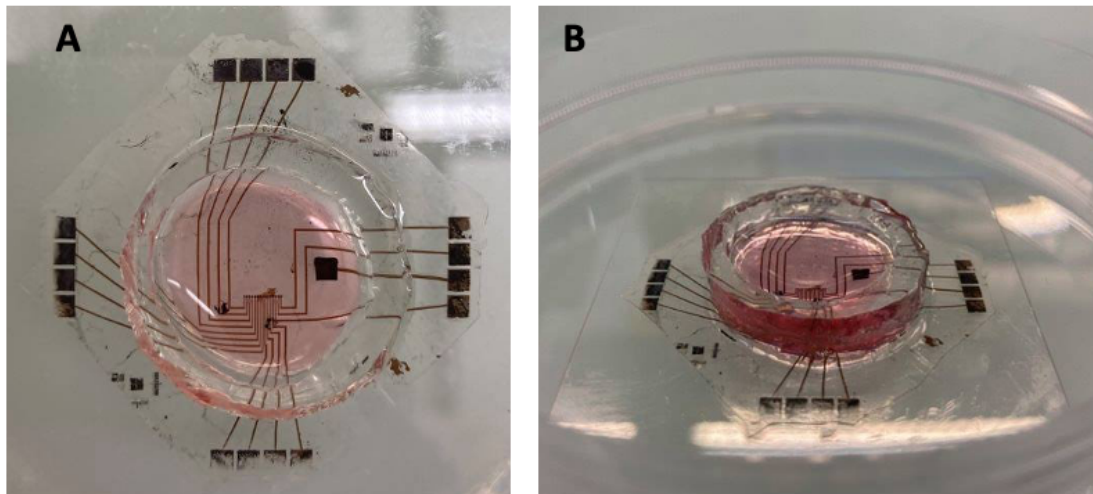


Figure 3.12: Completed Electrode Assembly. (A) Top view with the structure mounted on the electrodes. (B) Side view.

The final device that can be used for electrical stimulation experiments is shown in Figure ???. The microstructure-MEA assembly consists of the PDMS micro-structure aligned on top of the electrode tracks and a PDMS ring in the centre as a reservoir for coating solutions and cell medium.

3.7 Axonal Growth on Electrodes

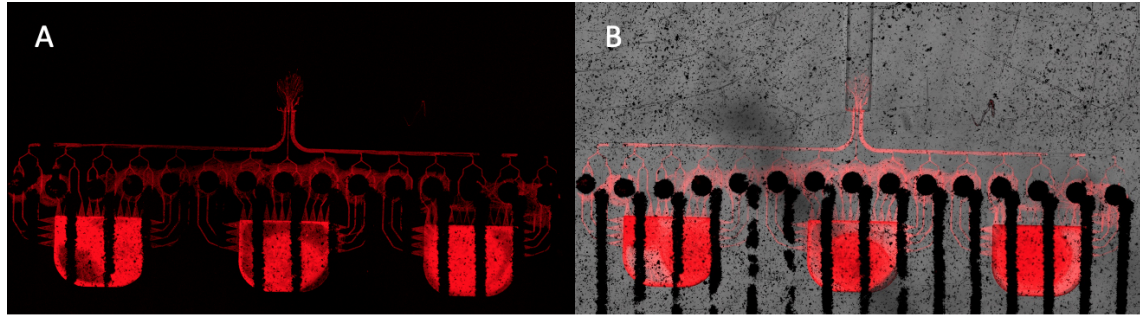


Figure 3.13: Axonal growth and confinement on gold nanowire (Au NW) electrodes at Day 5. (A) Red-channel image. (B) Merged image.

Figure ?? shows the axonal growth where the images were taken with an inverted CLSM. The axonal growth was refined inside the channels but axonal escape around the electrode pads was observed.

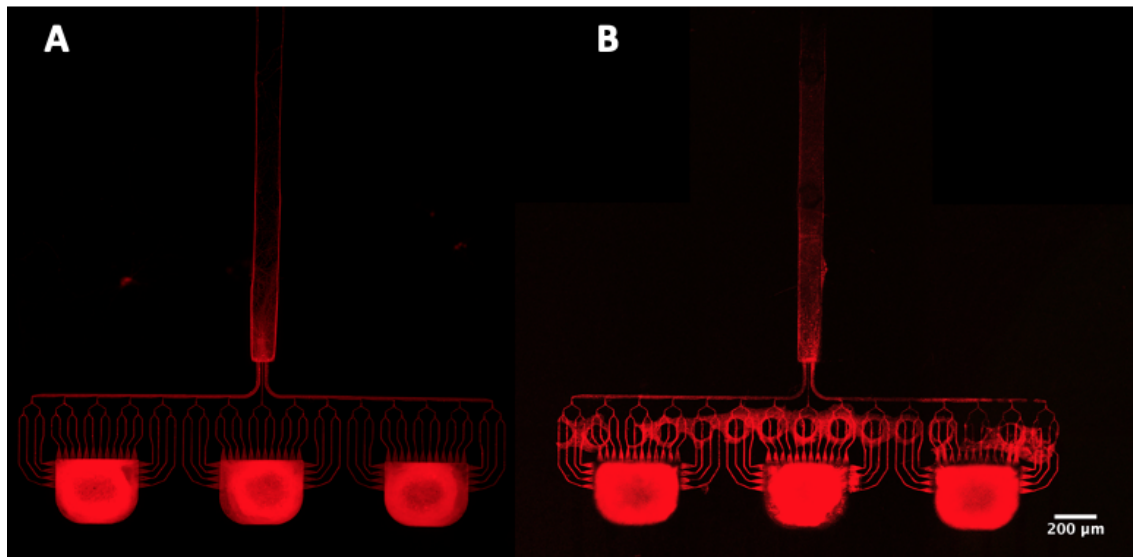


Figure 3.14: Axonal growth and confinement on glass control (A) and gold nanowire (Au NW) electrodes (B) at Day 10 in red channel imaged using an upright CLSM.

The same gold electrode shown in Figure ?? was also imaged at Day 10 using an upright CLSM set-up to image the top of the electrodes as shown in Figure ?? (B). Despite the escape of axons around the pads, the axons were growing in a refined manner inside the micro-channels that were aligned on top of the electrode pads in the centre.

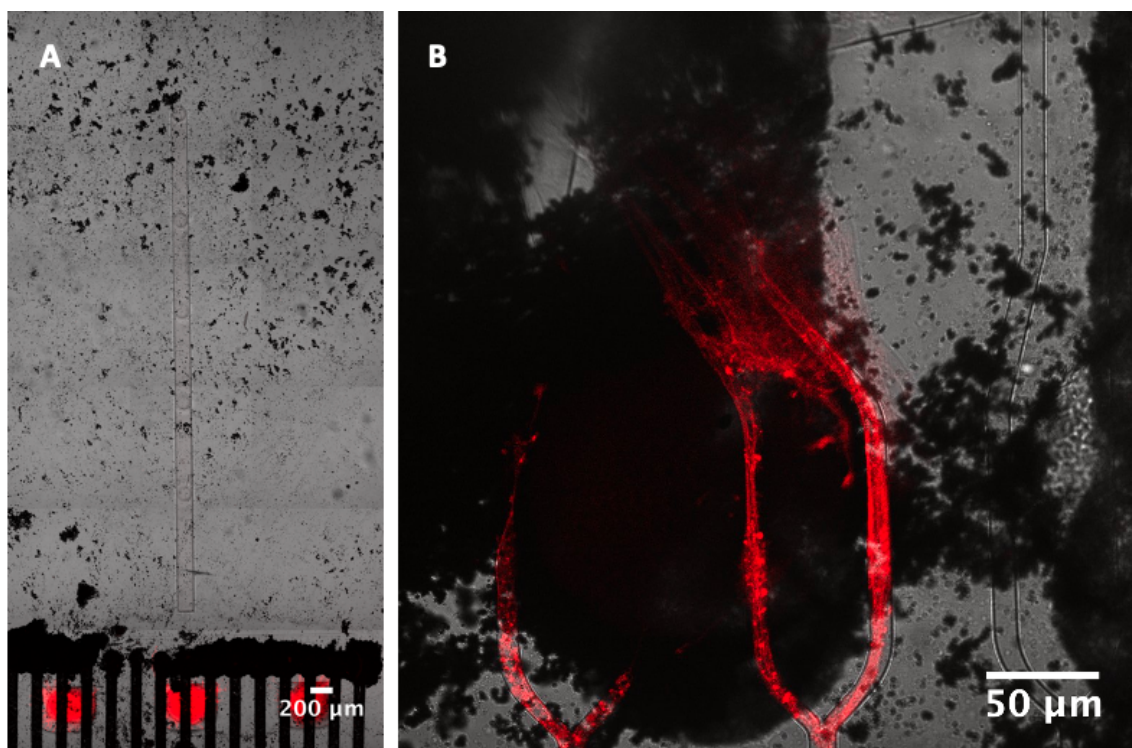


Figure 3.15: Axonal growth and confinement on platinium (Pt) electrodes. (A) Image taken with the inverted CLSM at Day 5 using a $\times 10$ lens. (B) Image taken with an upright CLSM at Day 10 using a $\times 40$ immersion lens.

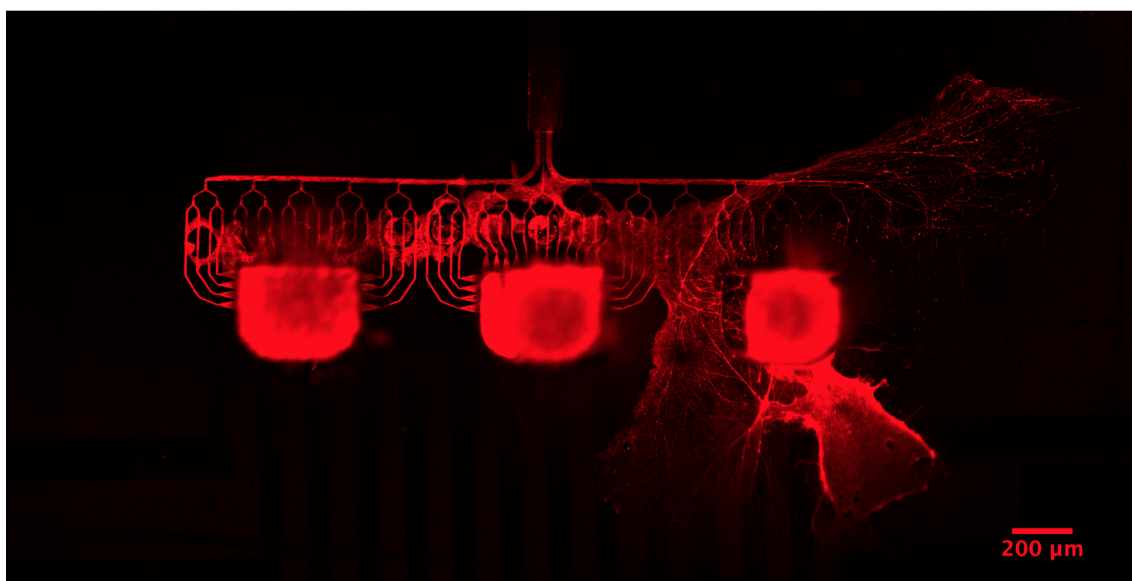


Figure 3.16: Image of axonal growth on the platinium electrode surface without the glue (control).

As shown in Figures ?? and ??, overall more axonal growth was observed in the gold nanowire electrodes. Moreover, the control experiment of the assembly on Pt electrodes without using any

glue shows escaping of the axons in Figure ???. A general observation made is the use of weights help improve the sealing of the microstructure-MEA assembly to help confinement of the axons.

3.8 Re-using Microstructure-MEA Assemblies

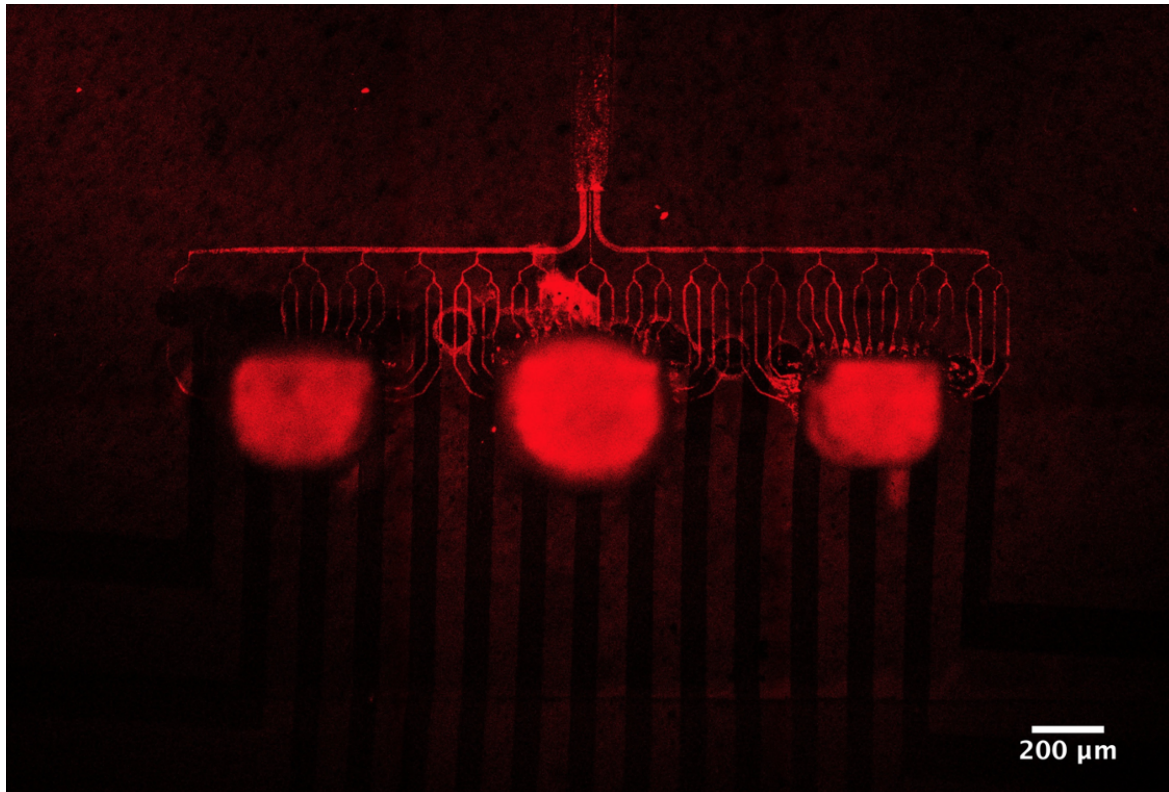


Figure 3.17: Axonal growth in a reused microstructure and gold nanowire (Au NW) electrodes assembly washed with 1% tergazyme.

Figure 3.8 demonstrates the feasibility of re-using the microstructure-MEA assembly using the protocol described in Section 2.13.

Chapter 4

Discussion

4.0.1 Significance and Interpretation of Results

Overall, the PDMS:Hexane glue dilution ratio of 1:40 found to be optimal for gluing the $6\mu\text{m}$ PDMS microstructures on top of the stretchable MEAs without clogging the channels. The t-peel test revealed that the 1:40 glue has a strain energy density as strong as thin film of uncured PDMS glue. On the other hand, PDL and laminin coating was found to be the most effective for promoting axonal growth based on % filled channels with axons, % surface area covered with axonal growth and distance travelled in the output channel. PDL and laminin coating by desiccation was found to be the best coating strategy for the micro-structure-MEA assembly which yielded % filled channels and % surface area covered with axonal growth similar to that of the Control PDL+laminin group. Finally, a procedure to precisely align, glue and seal PDMS microstructures on top of the electrode tracks using a custom set-up was developed. The final proof-of-concept stretchable device that resembles the conventional MEA systems can be used to perform stimulation experiments.

According to the results, 1:40 dilution was found to be the optimum as a trade-off between having a sufficient amount of PDMS in the glue dilution for stronger bonding and avoiding clogging of the channels. Moreover, there was no axonal escape observed in the glued structures. Reproducibility of the glue dilution was further evaluated by performing cell culture experiments which showed that out of 60, 58.95 ± 1.40 of the microchannels were open whereas 4.44 ± 4.56 of the junction channels were clogged. Overall, the 1:40 glue dilution yielded reproducible results although there were a small number of clogged channels which can potentially be explained by the glue re-flowing in to the channels due to capillary forces. In order to overcome this issue of glue flowing into the channels, the wafer can be pre-baked at a low temperature to increase viscosity before the stamping process. [?]) Alternatively, coggings can be a result of manual mounting which relies on steady hands and dexterity as well as the cleanliness of the wafer which suggests that more reliable gluing can potentially be achieved by using the mask aligner set-up in a clean room setting. The slight variations observed could potentially also be due to errors while pipetting viscous PDMS. Diluted PDMS glue is considered as an effective bonding compared to O₂ plasma bonding. Firstly, micro-channels assembled using μ TA/glue have been previously reported to have more defined

boundaries where the PDMS prepolymer can fill nanogratings on the rough surfaces providing an effective sealing thus preventing leakage. On the other hand, performance of the glue/ μ TA is more robust against contaminants such as dust whereas presence of dust can fail an O₂ plasma assembly. [?] Another drawback of O₂ plasma bonding is the reproducibility and reliability. [?] It's been previously reported that bonding strength of O₂ plasma assemblies can be subject to fluctuations up to 50 %. [?] [?] These arguments are also indicated in the results of the t-peel test where although the plasma bonding was stronger than the bonding with 1:40 PDSM:Hexane glue in one case, the other two cases failed leading to a strain energy density of 0. Also, glue/ μ TA technique can be performed using only a spin coater whereas O₂ plasma relies on a plasma generator. [?] Last but not least, performing plasma with the proposed alignment method may not be practical to implement since the plasma activated surfaces should be brought together as quickly as possible. On the other hand, the glue can further be improved in a number of ways. It's been previously reported in a number of studies that hexane can be used to dilute uncured PDMS in order to spin thin films. [?] However, hexane is known to swell cured PDMS. This can be avoided by using a longer spin coating time (>5mins, although data not widely available) or dilutions can be performed using tert-butyl alcohol which has been shown to be biocompatible. Alternatively, UV-PDMS after different exposure times can be tested.

No axonal growth was observed in the control PDMS group compared to the other treated groups which is most likely because of low cell attachment on the surface indicating that surface modifications are necessary for improved axonal growth inside the micro-channels as previously reported [?]. Although PDMS is an excellent material for microfluidics and stretchable electronics, the presence of organic methyl groups present in the chemical composition of PDMS makes the surface hydrophobic leading to poor wettability and weak cell attachment. Therefore, surface coating is indispensable to promote optimal cell adhesion by increasing hydrophilicity. Poor adhesion in turn leads to insufficient neurite outgrowth [?]. Based on the parameters assessed such as % filled channels, % growth area and distance travelled in the output channel to evaluate the success of the coating condition, control group coated with PDL+Laminin yielded considerably more growth at a faster rate compared to the Control PDL group. This finding is consistent with the results from the literature. [?] PDL and laminin coating has been widely used in neural cell cultures and scaffolds in numerous studies. [?] The difference observed between PDL and PDL+Laminin groups could be due to the fact that, although neural adhesion can be faster with more neurites on PDL coated surfaces, it's been shown that laminin can facilitate neuritogenesis more, therefore, can promote axonal guidance and growth of longer neurites and axonal guidance. [?] [?] In more detail, PDL is a positively charged synthetic polymer which can bind to the negatively charged PDMS. However, less biological activity have been reported on synthetic polymers as confirmed by the results of this study. [?] Polycations such as PDL are commonly combined with proteins such as laminin which is one of the typical components of the ECM help mimic the native ECM structure of the host as closely as possible and act as a biochemical cue to promote cell adhesion. [?] [?] [?] By this way, cells can adhere to laminin though their membrane receptors. Laminin has also been shown effective in inducing cell attachment in scaffolds as well. [?] For example, Peng et

al (2016) has reported a bio-scaffold coated with laminin for RPE implantation where the macular function was preserved up to 2 years *in vivo* [?] [?]. Therefore, two component coating with PDL and Laminin was chosen as the optimal coating for a favourable environment for cell adhesion and viability in the micro-channels.

Coating with PDL and laminin by desiccation after mounting of the structures yielded axonal growth similar to that observed to the PDL and laminin on glass control group in terms of % channels filled and % surface area covered by the axons. Moreover, control PDL+laminin on glass and coating by desiccation yielded reproducible results across different experiments and structures where axonal growth in each group was similar. However, distance travelled by the axons after coating by desiccation was significantly lower compared to the control PDL and laminin group which will be further discussed in the limitations of the study.

Substantially low growth was observed in the PDL on PDMS group. In addition, other groups did not facilitate axonal growth as much as in the control and coating by dessciation groups which can potentially be explained by the fact that coating can be affected by the heat or the glue flowing on to the surroundings and damaging the coating. Moreover, interaction between the coating agent and hexane as well as uncured PDMS is not known which can also potentially have a negative effect on the coating.

The observed decrease in the distance travelled in the output channel by the axons in the non-plasma groups after Day 22 indicate collapsing of the bundle meaning the cell attachment is unstable and not sustainable over long-term. This formation of an unstable bundle that collapses around after Day 22 in no plasma activation coatings whereas a distributed growth in the output channel in the plasma treated cases was consistently observed. This can potentially be explained by the fact that O₂ plasma treatment results in hydrophobic hydrocarbon groups (-CH₃) being replaced by hydrophilic silanol groups (SiOH) after oxidisation thus improving wettability. This increase in wettability in turn facilitates the adhesion of the coating material for a more sustainable cell attachment [?]. The downside of using plasma treatment is the hydrophobic recovery over time, which may not be suitable for long-term cultures. In addition, it should be noted that there has been a report where laminin when used together with oxygen plasma was less effective than other ECM proteins [?]. On the other hand, toluene washes were omitted from the protocol, as the swelling of the PDMS microstructures in a solvent such as toluene can lead to the distortion of the required microchannel dimensions [?].

A strength of this study is the use of primary cell cultures which are harvested from healthy animal tissues and compose of naive cells which can provide a realistic model of axon regeneration and behaviour *in vivo* compared to single cells [?]. The variability observed within the same experimental groups can be explained by a number of reasons. Overall, marginal changes and variations observed in axonal growth within the same groups over time, could be due to alterations in the chemical microenvironment (i.e. pH) and digestion by cells which result in changes in or degradation of the biochemical coating [?]. More importantly, although explants have a higher survival rate [?], cutting explants of similar size reproducibly is a challenge and the efficiency of the AAV transduction efficiency might be reduced since the virus needs to penetrate and infect

the whole explant rather than single cells. Therefore, using spheroids for the future experiments is likely to yield more reproducible results and result in more uniform viral tagging of the cells.

As indicated by the coating results, the heat treatment might have an adverse effect on the coating and slow down the axonal growth perhaps due to the denaturation of laminin at high degrees [?]. Furthermore, as mentioned before, the interaction of the uncured glue with the coating is yet unknown. The glue might flow onto the coating which can be detrimental to the coating. Due to these reasons and in order to minimise the potential damage to or drying of the coating during the alignment and mounting using the mask aligner, coating of the electrodes was done by desiccation after the structure have been aligned and mounted which yielded a similar growth pattern to control PDL+Laminin group. This also allows more flexibility during the alignment process and handling of the electrodes and mounting of the rings afterwards. Furthermore, having the structures already been mounted and cured before the coating offers the possibility of curing the glue overnight at 80 °C to make sure hexane between the two PDMS layers completely evaporates and the thin layer of glue fully cures. Moreover, ethanol or acetone can be used for sterilisation of the devices or to remove uncrosslinked oligomers prior to coating and cell seeding without the risk of damaging the coating. More importantly, for the next stage of the project where a collagen tube will be incorporated to the end of the channel, it is essential to coat the microfluidic channels after the mounting process has been completed which might otherwise lead to drying of the collagen tube at high degrees.

The gluing technique makes it more challenging to perform alignment on the electrodes since moving the stamped structure on the electrode surface can lead to the glue being smeared around which in turn might clog the channels. The proposed alignment method makes it possible to perform alignment and seal the structure on top of the electrodes in one go, reducing the risk of channels being clogged by the glue being smeared around. Moreover, the method offers a precise and a more reproducible way of aligning since it's less dependent on dexterity and hand alignment thus minimising human error that can be caused by unsteady hand motions. Overall, the feasibility of the proposed assembly method as well as the biocompatibility of microstructure-MEA assembly was confirmed by culturing cortical nerves on top of the electrodes. Weights were added to apply a slight pressure to make sure that there are no visible voids due to variable surface flatness of the MEA surface.

Explanation for the difference between nanowire Au and Pt could be that the surface roughness might be different. The exposed parts of the nanowires embedded in PDMS can act as nano topography cues and promote cell adhesion. Alternatively culture on Pt electrodes can be improved by pre-culturing the electrodes with cells to make sure anything that might be toxic for the cells has been cleared out and the second culture can yield better growth due to residual cell debris [?]. Moreover, the irreversible bonding and washing protocol using tergazyme makes it possible to re-use the stretchable MEAs instead of repeating the gluing and re-alignment process. This can make the stimulation experiments less time-consuming in the future and keep the alignment consistent with each experiment.

4.0.2 Limitations and Future Work

The study has a number of limitations. First of all, all the coating experiments were performed with triplicates which reduces the statistical power considering the biological variation observed. On the other hand, a new challenge introduced by the proposed coating method, PDL+Laminin by desiccation after mounting, is that the surface of the PDMS microstructures is coated as well. This results in axons growing also on top of the surface instead of only inside the channels which can potentially explain why the distance travelled in the output channel in the groups coated by desiccation is lower compared to the control PDL+Laminin group. In order to circumvent this difficulty in the final device, an anti-fouling coating agent such as PMOXA [?] or a mask on the surface of the PDMS microstructure can be used. Another explanation could be due to the wash steps after the PDL coating. Despite 10 minutes wait in between every wash step and re-desiccation and incubation with laminin overnight, it might be likely that a small amount of the PDL solution remains inside the channels and doesn't diffuse out. As mentioned previously, any residual non-physisorbed PDL fragments trapped in the microchannels after the PDL washing procedure can be toxic to the cells. Moreover, as indicated by the results of the coating experiment, a higher intensity was measured at the beginning of the channel which can either be due to residual PDL left inside the channel or the beginning of the channel having a thicker PDL coating. This potential issue can systematically be checked by first coating the surface with normal PDL followed by coating with fluorescent PDL and performing a time lapse experiment to be able to determine the time it takes to completely wash off the fluorescent PDL from the microchannels. It is critical to first perform the coating using PDL in order to avoid fluorescent PDL coating the surface and make sure it remains in the microchannels so that the washing off can be tracked. Otherwise it becomes challenging to differentiate between the PDL coating and PDL inside the microchannels if fluorescent PDL is used directly. Another possible explanation could be the pH changes during the desiccation step affecting the coating.

There are also certain limitations associated with assessing the bonding strength measurements. T-peel test might not represent the actual forces the implant will be exposed to after implantation to the brain. This makes it challenging to compare the bonding numerically with literature to be able to accurately judge if the bonding is strong enough to endure the implantation and forces exerted through micro-motions after conforming on the brain without failing [?]. Other tests that can be used to confirm the bonding strength and further characterisation in a scenario that better mimics and reproduces the forces in the brain include lap-shear tests and bulge tests on the assembly itself [?] [?]. The bonding strength with the electrode surface should also be assessed directly on the electrode surface rather than plain PDMS. This is because the surface properties and roughness of the electrode surface so does the bonding could be different. Alternatively, the PDMS micro-structure can be filled with dye and the channels can be observed for leakage while the assembly is under cyclic tensile stretching or bending.

There are also several features that can be improved in the design of the structures. In order to improve and speed up the alignment procedure, alignment marks can be added to the structures.

Moreover, the micro-channels can be re-designed to be wider to facilitate more efficient diffusion and exchange of nutrients, make it possible to use a lower dilution ratio of PDMS without clogging the channels and to make the design more tolerable to misalignment.

For the bundling analysis, although the Gaussian fit method can provide a numerical insight regarding the degree of bundling, it has a number of limitations. In cases, where there are more than one small bundles or when the axons are growing on the edges, the Gaussian fit becomes sub-optimal. In order to make the analysis more robust to such cases and biological variations, diffusion gradients can be calculated to evaluate axonal bundling where neuron tips are taken as diffusion sources in free space to derive the growth direction and elongation of neurites. This method is similar to diffusion tensor imaging which shows axonal bundling of fiber tracts in the real brain. [?]. Alternatively, data can be fit using a multi Gaussian fit to better account for the presence of individual axon bundles and detect two separate peaks for the cases where the axons grow on the output channel walls. Last but not least, bundling analysis can be carried out using a point density function which can potentially identify the spreadness of growth specially in plasma cases more accurately. [?]

To further promote axonal outgrowth and neural adhesion, hydrogels can be incorporated into the microchannels. Hydrogel filling is commonly adapted in biomaterial-based scaffolds used in vivo axonal regeneration [?]. Annabi et al. previously reported a method for hydrogel coating of microfluidic channels using a microfluidic set-up where a photocrosslinkable hydrogel was crosslinked under continuous flow inside the channels using UV light [?]. A similar strategy can be adapted in order to reinforce axonal growth inside the channels, particularly in the output channel, of the devices. On the other hand, although, axonal growth was confined inside the microchannels, axonal escape was observed around the edges of the electrode pads.

Although, alignment and cell confinement using the gluing and alignment described have been shown to be feasible and promising, the procedure should be tested with a larger number of microstructure-MEA assemblies in order to be able to derive statistical conclusions regarding the reproducibility of the proposed method. On the other hand, in order to further improve the cell confinement, the electrode pads can be better embedded by patterning selective openings through a photoresist lift-off technique as described by Park et al. [?]. Alternatively, weights lower than 5g can be used during the curing of the assembly to further seal the bonding between the electrode surface and the PDMS microstructure.

The next step of the project will be to demonstrate that the MEA-microstructure composite electrode can be used to stimulate neurons. This can be done by electrical stimulation of the individual channels or wells and measuring neuronal activity using Calcium imaging. The alignment and tangency of the electrode pads to the microchannels or wells can also be optimised via stimulation experiments. The effect of coating thickness might need to be investigated in order to achieve a high signal to noise ratio during recordings or stimulations.

Chapter 5

Conclusion and Outlook

To conclude, PDMS was diluted in hexane in order to spin-coat a thin layer of glue. The optimal dilution that would reproducibly confine axonal growth without clogging the channels was found to be 1:40 PDMS:Hexane. The ideal coating strategy was chosen to be PDL and laminin coating by dessication after the gluing of the PDMS microstructures on top of the electrodes. The coating still has a few minor challenges such as axons not travelling as far in the output channel or the surface of the structures being coated as well. In order to overcome such issues, the surface of the micro-structure can be masked during the coating or a micro-fluidic set-up can be used for the coating procedure. Last but not least, the feasibility of aligning and gluing of the PDMS micro-structures on top of MEA tracks using an alignment set-up has been demonstrated. In order to further improve the cell confinement around the electrodes, the electrode pads can be better embedded by patterning selective openings through a photoresist lift-off technique during the fabrication process. The final assembly of the stretchable microstructure-MEA prototype device that resembles the conventional MEAs will be used for the electrical stimulation experiments.

List of Figures

Please wait...

If this message is not eventually replaced by the proper contents of the document, your PDF viewer may not be able to display this type of document.

You can upgrade to the latest version of Adobe Reader for Windows®, Mac, or Linux® by visiting http://www.adobe.com/go/reader_download.

For more assistance with Adobe Reader visit <http://www.adobe.com/go/acrreader>.

Windows is either a registered trademark or a trademark of Microsoft Corporation in the United States and/or other countries. Mac is a trademark of Apple Inc., registered in the United States and other countries. Linux is the registered trademark of Linus Torvalds in the U.S. and other countries.